

# From classical to quantum non-equilibrium dynamics of Rydberg excitations in optical lattices

Marco Mattioli<sup>1,2</sup>, Alexander W. Glätzle<sup>1,2</sup> and Wolfgang Lechner<sup>1,2</sup>

<sup>1</sup>Institute for Quantum Optics and Quantum Information of the Austrian Academy of Sciences, A-6020 Innsbruck, Austria

<sup>2</sup>Institute for Theoretical Physics, University of Innsbruck, A-6020 Innsbruck, Austria

E-mail: marco.mattioli@uibk.ac.at

**Abstract.** The glass phase and its quantum analog are prominent challenges of current non-equilibrium statistical mechanics and condensed matter physics. As a model system to study the transition from classical to quantum glassy dynamics, we propose a setup of laser driven three-level atoms trapped in an optical lattice. Tuning the strength of the laser driving to the intermediate level allows one to study the transition from a classical Kinetically Constrained Model to the coherent regime. For strong driving, Rydberg excitations evolve analogously to defects in the One-Spin Facilitated Model, a minimal model known to exhibit glassy dynamics. In our setup, the constraints result from the interplay between Rydberg interactions and the laser detuning from the Rydberg state. The emerging heterogeneous relaxation timescales are tuneable over several orders of magnitudes. In the opposite limit of weak driving of the intermediate level, we find an effective cluster model which describes the dynamics in a reduced subspace of the allowed number and positions of Rydberg excitations. This subspace is uniquely determined by the initial state and is characterized by a fixed number of clusters of Rydberg excitations. In addition, we investigate the influence of random fields on the classical relaxation. We find that the glassy dynamics can relax faster in the presence of weak random fields.

## 1. Introduction

When disordered materials are quenched to low temperatures the dynamics can become non-ergodic and the system may fall out of equilibrium [1, 2, 3, 4, 5]. Understanding this phenomenon, known as the glass transition, is one of the open questions in current statistical mechanics. While a complete theory which satisfactorily explains all features of glass forming materials is missing, spin models have been proposed to understand particular aspects of the glass problem. For example, static properties of glasses are captured by Ising models with random interactions, the so-called spin glasses [6, 7, 8]. These models have recently gained renewed interest in the context of both quantum adiabatic optimization [9, 10] and, in presence of external random fields, of the many-body localization phase transition [11, 12, 13, 14]. Spin models which study dynamical properties of glasses are so-called Kinetically Constrained Models [15] (KCMs). In these KCMs, separation of relaxation timescales as well as space-time dynamical heterogeneities [5, 16] result from constrained transitions (spin flips) that are allowed or forbidden depending on the state of neighboring spins. Quantum effects in KCMs have been recently studied in Refs. [17, 18, 19, 20, 21] in ultracold Rydberg atoms. Thanks to their strong and long-range interactions, as well as to their long lifetimes [22, 23, 24], Rydberg atoms offer a promising framework to study quantum spin models in- and out-of-equilibrium [25, 26, 27, 28, 29, 30, 31, 32, 33, 34, 35, 36]. With the considerable recent experimental development in atomic, molecular and optical physics, Rydberg atoms can in fact be trapped, laser-excited and detected with single particle resolution in state-of-the-art experiments [37, 38, 39, 40, 41, 42, 43, 44].

In this work we propose a model system based on V-shaped three-level atoms, where each atom is resonantly driven from its electronic ground-state  $|g\rangle$  to a short-lived low-lying excited state  $|e\rangle$  and far-off-resonantly driven to a metastable Rydberg state  $|r\rangle$  (see Fig. 1). Here, tuning the driving strength  $\Omega_e$  of the  $|g\rangle \leftrightarrow |e\rangle$  transition, allows one to study the crossover from classical to quantum dynamics of the Rydberg excitations. For strong driving, the relaxation of Rydberg excitations resembles the one of defects in a classical KCM, the One-Spin Facilitated Model [15, 18] (1-SFM). In this setup, kinetic constraints are a consequence of the interplay between strong interactions of Rydberg-excited atoms [45] and the laser detuning from  $|r\rangle$ . In contrast, for vanishing  $\Omega_e$ , coherences of the  $|g\rangle \leftrightarrow |r\rangle$  transition dominate the dynamics within the lifetime of the Rydberg states [37]. In the case of large laser detuning from the Rydberg state, the system explores only a reduced subspace of the total Hilbert space, which is determined by the initial state. We present an effective simple model to describe the evolution in this regime which is based on a fixed number of Rydberg clusters. Finally, we study the interplay between internal dynamical constraints and external disorder arising from random fields. Here, random fields can be implemented using static site-dependent random detunings from the Rydberg state. Our results indicate that the glassy relaxation of Rydberg excitations toward the steady state can be accelerated by the presence of weak random fields.

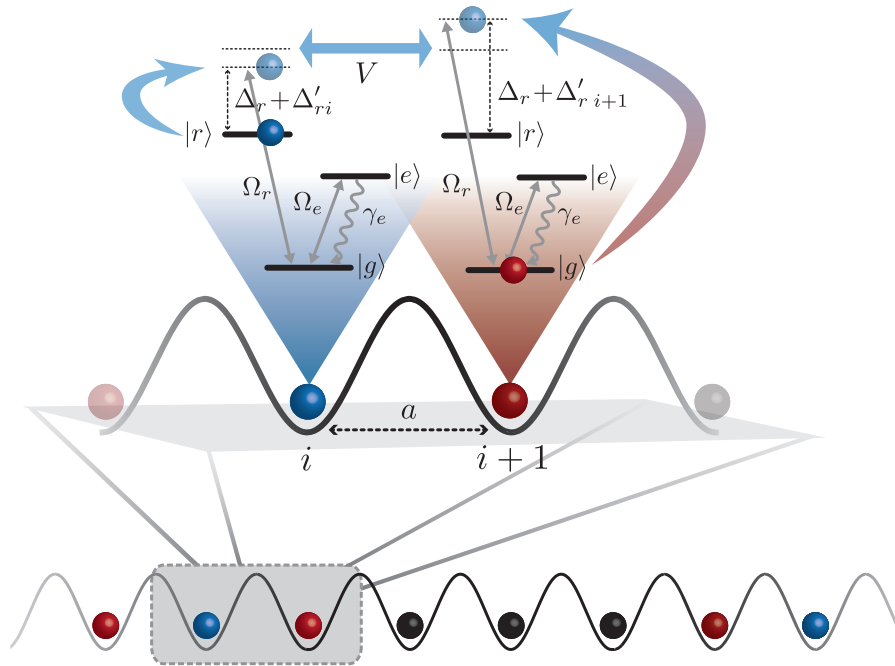


**Figure 1.** The setup we have in mind consists of three-level atoms, each one schematized with a ground-state  $|g\rangle$ , a Rydberg state  $|r\rangle$  and an intermediate excited state  $|e\rangle$ . Atoms are coherently laser-driven with Rabi frequencies  $\Omega_e$  ( $\Omega_r$ ) between  $|g\rangle$ - $|e\rangle$  ( $|g\rangle$ - $|r\rangle$ ) and  $\gamma_e$  is the decay rate due to spontaneous emission from  $|e\rangle$ . The anti-blockade condition  $V = \Delta_r$ , i.e. when the laser detuning  $\Delta_r$  with respect to the  $|g\rangle$ - $|r\rangle$  atomic transition is equal to the interactions between neighbouring Rydberg-excited atoms  $V$  (see Subsec. 2.2), ensures that whenever an atom is in  $|r\rangle$  (*defect*, blue sphere), an atom next to it, initially in  $|g\rangle$  (*facilitated* atom, red sphere), will also be favoured to be excited to  $|r\rangle$ . An atom in  $|g\rangle$  far from a defect (*non-facilitated* atom, black sphere) is blocked, because its  $|g\rangle$ - $|r\rangle$  transition is far-off-resonant (see Subsec. 4.1). The case with additional site-dependent random detunings  $\Delta'_{ri}$  is studied in Subsec. 4.3.

The remainder of the paper is organized as follows: In Sec. 2 the level-scheme and the model are introduced; in Sec. 3 we give a brief overview of SFMs. Numerical results from quantum trajectory simulations are presented in Sec. 4. In Subsec. 4.2 we study the coherent regime and the transition to the rate equation limit and in Subsec. 4.3 we analyze the case of finite random detunings from the Rydberg state. The validity of the assumptions and approximations of Sec. 4 are discussed in Sec. 5. Finally, in Sec. 6 we summarize our conclusions.

## 2. Model

We consider  $N$  atoms individually trapped in a one-dimensional (1d) large spacing optical lattice [37, 46, 47, 48, 49] or in a magnetic trap array [50, 51]. Atomic motion due to tunnelling between adjacent sites is negligible within experimental timescales. Each atom is approximated as a three-level system in the V-configuration, as schematically depicted in Fig. 1: the electronic ground-state  $|g\rangle$  is laser driven to (i) a Rydberg state

$|r\rangle$  with a small Rabi frequency  $\Omega_r$ , and (ii) to an excited state  $|e\rangle$  with a large Rabi frequency  $\Omega_e$ . The intermediate low-lying excited state  $|e\rangle$  is rapidly decaying to  $|g\rangle$  and its short lifetime is given by the inverse of the decay rate  $\gamma_e$ . Two atoms in their Rydberg states interact via dipole-dipole  $V(x) = V/x^3$  or van der Waals  $V(x) = V/x^6$  potentials, depending on the presence or absence of an applied external field [23], respectively. We approximate interactions between Rydberg-excited atoms to be nearest-neighbor, i.e.  $V(1) = V$  and  $V(x \geq 2) = 0$ . Results under this assumption are in qualitative good agreement with simulations of the full model including long-range interactions (see Sec. 5). Furthermore, we neglect processes of spontaneous emission from the Rydberg state, setting the associated rate  $\gamma_r$  to zero. Limitations of the validity of this approximation are discussed in detail in Sec. 5.

The Hamiltonian in the rotating frame with  $\hbar = 1$  is

$$\begin{aligned}
 H = \sum_{i=1}^N \left\{ \frac{\Omega_e}{2} (|g\rangle\langle e|_i + \text{H.c.}) + \frac{\Omega_r}{2} (|g\rangle\langle r|_i + \text{H.c.}) + \right. \\
 \left. - (\Delta_r + \Delta'_{ri}) |r\rangle\langle r|_i \right\} + V \sum_{i=1}^{N-1} \left\{ |r\rangle\langle r|_i \otimes |r\rangle\langle r|_{i+1} \right\}. \quad (1)
 \end{aligned}$$

Here, the sum runs over all lattice sites  $i$ , while  $\Delta_r$  and  $\Delta'_{ri}$  are the homogeneous and site-dependent random laser detunings from  $|r\rangle$ , respectively. The random detuning can, for example, be induced by a spatially inhomogeneous ac-Stark shift acting on the Rydberg- or ground-state using either a random light pattern or differential light-shifts between atoms in different traps, in close analogy to experiments performed in the context of Anderson localization [52, 53].

### 2.1. A single-atom in the $V$ -configuration

Let us first review the properties of a single three-level atom in the special case of resonant Rydberg excitation and zero random detuning, i.e.  $\Delta_r = \Delta'_{ri} = V = 0$ . In this case, the Hamiltonian of Eq. (1) reduces to

$$H = \frac{\Omega_e}{2} (|g\rangle\langle e| + \text{H.c.}) + \frac{\Omega_r}{2} (|g\rangle\langle r| + \text{H.c.}). \quad (2)$$

In the Born-Markov approximation, the master equation describing the evolution of the reduced system density matrix  $\rho(t)$  is in the Lindblad form

$$\dot{\rho}(t) = -i[H, \rho(t)] + \frac{\gamma_e}{2} (2c\rho(t)c^\dagger - c^\dagger c\rho(t) - \rho(t)c^\dagger c), \quad (3)$$

where  $c = |g\rangle\langle e|$  is the quantum jump operator [54].

Under continuous monitoring of the strong transition  $|g\rangle \leftrightarrow |e\rangle$  with a photodetector and during time intervals where no photons are detected, the system wave function  $|\psi(t)\rangle$  evolves according to the Schrödinger equation  $i\frac{d}{dt}|\psi(t)\rangle = H_{\text{eff}}|\psi(t)\rangle$ , with

$$H_{\text{eff}} = H - \frac{i\gamma_e}{2} c^\dagger c = H - \frac{i\gamma_e}{2} |e\rangle\langle e| \quad (4)$$

an effective non-Hermitian Hamiltonian. The general solution for the system wave function is

$$|\psi(t)\rangle = \sum_{n=1}^3 c_n e^{-i\lambda_n t} |u_n\rangle, \quad (5)$$

where  $\lambda_n$  and  $|u_n\rangle$  are the eigenvalues and associated eigenvectors of  $H_{\text{eff}}$ , respectively [55]. The coefficients  $c_n$  can be determined from the initial condition, e.g.  $|\psi(0)\rangle = |g\rangle$ . In Appendix A we compute  $\lambda_n$  and  $|u_n\rangle$ , using the Brillouin-Wigner perturbation theory in the limit  $\Omega_r \ll \Omega_e, \gamma_e$ . The eigenvalues  $\lambda_n$  are complex numbers all with negative imaginary parts  $\text{Im}\{\lambda_n\}$  and, as a consequence,  $|\psi(t)\rangle$  does not conserve the norm during the evolution. Moreover, for  $\Omega_r \ll \Omega_e^2/\gamma_e$ , one of the eigenvalues of  $H_{\text{eff}}$ , denoted by  $\lambda_3$ , has a much less negative imaginary part with respect to the other two,  $|\text{Im}\{\lambda_3\}| \ll |\text{Im}\{\lambda_1\}|, |\text{Im}\{\lambda_2\}|$  [55]. This determines long tails in the delay function

$$D_0(t) = \sum_{n=1}^3 |c_n|^2 e^{2t\text{Im}\{\lambda_n\}}, \quad (6)$$

defined as the conditional probability that no photon has been detected until time  $t$ , given a photon count has occurred at  $t = 0$ . Note that  $D_0(t)$  is exactly the norm of  $|\psi(t)\rangle$ , and its monotonous decay is dominated, in the long time limit, by  $\text{Im}\{\lambda_3\}$ . Thus,  $\text{Im}\{\lambda_3\}$  is responsible of the existence of a small but finite probability of a long time window with no photon counts. When such a long interval of no photon counts occurs, the atom is prepared in the Rydberg state and  $|\psi(t)\rangle$  is dominated by  $|u_3\rangle$ , which in turn can be expressed as  $|r\rangle$  plus a perturbatively small admixture of  $|g\rangle$  and  $|e\rangle$  (see Appendix A).

Trajectories  $|\tilde{\psi}_\alpha(t)\rangle$ , can be simulated using the quantum jump method described in Appendix B (see also Refs. [56, 57]). The index  $\alpha$  labels the  $N_{\text{traj}}$  stochastically independent trajectories. A typical experimental sequence of photon detections is an alternation of *bright* and *dark* periods. During a *bright* period the atomic population is rapidly cycled between  $|g\rangle$  and  $|e\rangle$  and the time between two successive photon detections is of the order of the lifetime of  $|e\rangle$ ,  $\gamma_e^{-1}$ . In contrast, during a *dark* period, the atomic population is shelved in  $|r\rangle$  and no photons are detected. An approximation of the exact time evolution of  $\rho(t)$  governed by Eq. (3) is generated by repeating the algorithm in Appendix B for  $N_{\text{traj}}$  trajectories and finally averaging over them, such that

$$\rho(t) = \lim_{N_{\text{traj}} \rightarrow \infty} \frac{1}{N_{\text{traj}}} \sum_{\alpha=1}^{N_{\text{traj}}} |\tilde{\psi}(t)\rangle_\alpha \langle \tilde{\psi}(t)|. \quad (7)$$

In the following, the observable we are interested in is the Rydberg population, that is, the expectation value of the Rydberg projector  $|r\rangle\langle r|$  in  $|\tilde{\psi}(t)\rangle_\alpha$ ,

$$r_\alpha(t) = ||\langle r|\tilde{\psi}(t)\rangle_\alpha|^2. \quad (8)$$

Averaging  $r_\alpha(t)$  over  $N_{\text{traj}}$  leads to

$$R(t) = \frac{1}{N_{\text{traj}}} \sum_{\alpha=1}^{N_{\text{traj}}} r_\alpha(t). \quad (9)$$

In analogy to Eq. (7),  $\lim_{N_{\text{traj}} \rightarrow \infty} R(t) = \rho_{rr}(t)$ , where  $\rho_{rr}(t) \equiv \langle r | \rho(t) | r \rangle$  is the Rydberg population whose evolution is governed by Eq. (3). Fig. 2 shows that  $R(t)$  converges to  $\rho_{rr}(t)$  by increasing  $N_{\text{traj}}$ . Due to the telegraphic behaviour of the photodetector

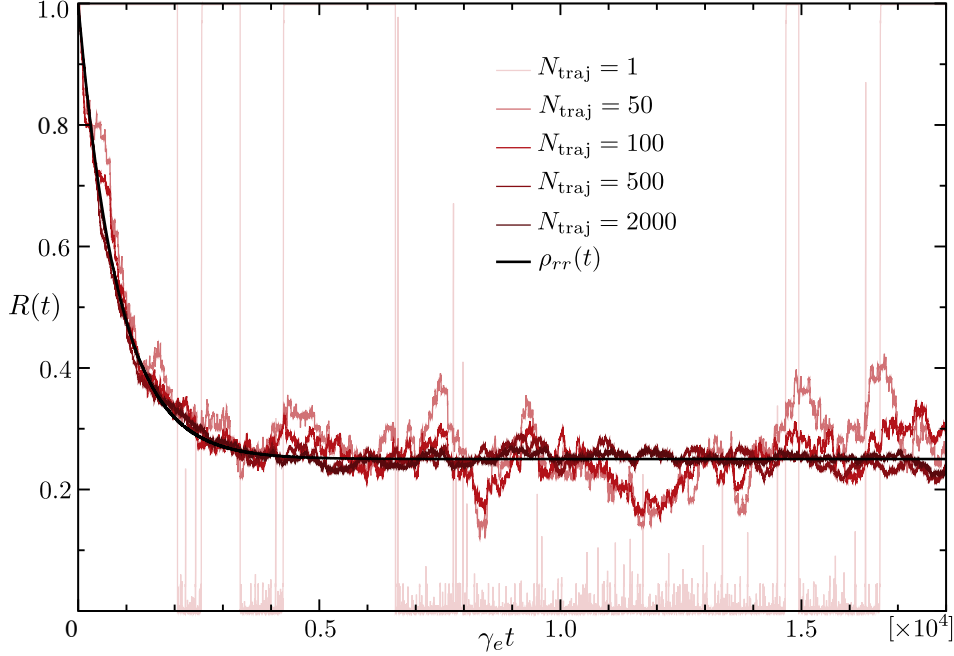


**Figure 2.** Rydberg population  $R(t)$  averaged over  $N_{\text{traj}}$  trajectories compared to the exact evolution  $\rho_{rr}(t)$  governed by Eq. (3). Parameters are:  $\Omega_e = \gamma_e$  and  $\Omega_r = 0.03\gamma_e$ . Increasing  $N_{\text{traj}}$ ,  $R(t)$  converges to  $\rho_{rr}(t)$ , as expected.

signal, *bright* and *dark* periods can be encoded in two classical spin variables 0 and 1, respectively. We denote the average duration of a *bright* and *dark* period with  $T_0$  and  $T_1$ , respectively.

In the following we illustrate three independent methods for the estimation of  $T_0$  and  $T_1$ , or equivalently of the transition rates  $\Gamma^{0 \rightarrow 1} \equiv T_0^{-1}$ , and  $\Gamma^{1 \rightarrow 0} \equiv T_1^{-1}$ . In Ref. [58], these rates are expressed as

$$\Gamma^{0 \rightarrow 1} = \left. \frac{d\rho_{rr}(t)}{dt} \right|_{t=0}, \quad (10)$$

together with  $\rho_{rr}(0) = 0$ , and

$$\Gamma^{1 \rightarrow 0} = - \left. \frac{d\rho_{rr}(t)}{dt} \right|_{t=0}, \quad (11)$$

together with  $\rho_{rr}(0) = 1$ . Consequently, transition rates can be extracted by linearization of the short-time evolution of  $\rho_{rr}(t)$  with the proper initial condition (e.g., from Fig. 2, we can estimate  $\Gamma^{1 \rightarrow 0}$ ).

For comparison, we calculate analytically the rates as follows: in the long time limit  $D_0(t) \sim p e^{-t/T_1}$ , where  $p$  is the (small) probability to be in a *dark* period [59, 60].

Comparing it with Eq. (6) we obtain

$$\Gamma^{1 \rightarrow 0}(\Delta_r) = -2 \operatorname{Im}\{\lambda_3\} = \frac{\gamma_e \Omega_e^2 \Omega_r^2}{16\Delta_r^4 + 4\Delta_r^2(\gamma_e^2 - 2\Omega_e^2) + \Omega_e^4}, \quad (12)$$

and

$$p = |c_3^2| = \frac{\Omega_r^2(\gamma_e^2 + 4\Delta_r^2)}{16\Delta_r^4 + 4\Delta_r^2(\gamma_e^2 - 2\Omega_e^2) + \Omega_e^4}, \quad (13)$$

where both results are obtained from  $\lambda_3$  and  $c_3$  calculated in [Appendix A](#) under the general assumption  $\Delta_r \neq 0$ . In order to compute  $\Gamma^{0 \rightarrow 1}(\Delta_r)$ , we note that, during a *bright* period,  $|r\rangle$  is almost never populated and the effective emission rate will be that of the (resonantly driven) two-level system  $|g\rangle \leftrightarrow |e\rangle$ , i.e.  $\gamma_e \Omega_e^2 / (\gamma_e^2 + 2\Omega_e^2)$ . Then,  $\Gamma^{0 \rightarrow 1}(\Delta_r)$  is simply the two-level emission rate multiplied by  $p$  [55],

$$\Gamma^{0 \rightarrow 1}(\Delta_r) = \frac{\gamma_e \Omega_e^2 \Omega_r^2 (\gamma_e^2 + 4\Delta_r^2)}{(\gamma_e^2 + 2\Omega_e^2)[16\Delta_r^4 + 4\Delta_r^2(\gamma_e^2 - 2\Omega_e^2) + \Omega_e^4]}. \quad (14)$$

When  $\Delta_r = 0$ , Eqs. (12) and (14) simplify to

$$\Gamma^{1 \rightarrow 0}(0) = \Gamma^{1 \rightarrow 0} = \frac{\gamma_e \Omega_r^2}{\Omega_e^2} \quad \text{and} \quad \Gamma^{0 \rightarrow 1}(0) = \Gamma^{0 \rightarrow 1} = \frac{\gamma_e^3 \Omega_r^2}{\Omega_e^2 (\gamma_e^2 + 2\Omega_e^2)}. \quad (15)$$

A third independent method relies on the direct calculation of the average over trajectories of the time-averaged length of *dark* and *bright* periods in each trajectory. Results for  $\Gamma^{1 \rightarrow 0}$ , obtained with the three different methods, are compared in [Tab. 1](#):

	<i>ME</i>	<i>PT</i>	<i>QT</i>
$\Gamma^{1 \rightarrow 0} / \gamma_e$	$9.02 \cdot 10^{-4}$	$9.00 \cdot 10^{-4}$	$9.13 \cdot 10^{-4}$

**Table 1.** Estimates of the resonant [ $\Delta_r = 0$ ] rate  $\Gamma^{1 \rightarrow 0}$  (in units of  $\gamma_e$ ), according to: the short time slope of  $\rho_{rr}(t)$ , obtained as the exact solution of the master equation (*ME*) [Eq. (3)], perturbation theory (*PT*) [Eq. (15)] and quantum trajectory simulations (*QT*) (see main text). In all three methods, parameters are:  $\Omega_e = \gamma_e$  and  $\Omega_r = 0.03\gamma_e$ . In the *QT* method, simulations of  $N_{\text{traj}} = 6000$  trajectories up to times  $\gamma_e t = 10^6$  are performed.

We find a good agreement, provided the condition of well-defined quantum jumps  $\Omega_r \ll \Omega_e^2 / \gamma_e$  holds, as it is the case within our parameter choice.

## 2.2. Many-body model

In the following we study the many-body model  $\Delta_r, V \neq 0$  without random detunings, i.e.  $\Delta'_{ri} = 0$ . The corresponding effective non-Hermitian Hamiltonian becomes

$$H_{\text{eff}} = H - \frac{i\gamma_e}{2} \sum_{i=1}^N |e\rangle\langle e|_i, \quad (16)$$

where  $H$  is given by Eq. (1) with  $\Delta'_{ri} = 0$ . Accordingly, the master equation reads

$$\dot{\rho}(t) = -i[H, \rho(t)] + \frac{\gamma_e}{2} \sum_{i=1}^N (2c_i \rho(t) c_i^\dagger - c_i^\dagger c_i \rho(t) - \rho(t) c_i^\dagger c_i), \quad (17)$$

and  $c_i = |g\rangle\langle e|_i$  is the quantum jump operator at site  $i$ . Furthermore, let us assume: (i)  $\Omega_r \ll \Omega_e^2/\gamma_e$ , as in Subsec. 2.1, for well defined quantum jumps to occur and (ii)  $V = \Delta_r$ , which we call the *anti-blockade* condition. The many-body transition rates can be determined as follows. In our  $1d$  system, due to the assumption  $V(x \geq 2) = 0$ , every process at a certain site can be influenced at most by its two nearest-neighbors. The many-body rates related to site  $i$  are obtained from Eqs. (12) and (14) with  $\Delta_r^* = \Delta_r - \ell V$ , where  $\ell \in [0, 2]$  labels the number of neighbors of  $i$  that are in the Rydberg state. Due to the *anti-blockade* condition, there are three possible configurations:  $\Delta_r^* = \Delta_r$  if there are no neighbors in the Rydberg state ( $\ell = 0$ ),  $\Delta_r^* = 0$  if there is only one neighbor in the Rydberg state ( $\ell = 1$ ) and  $\Delta_r^* = -\Delta_r$  if both neighbors are in the Rydberg state ( $\ell = 2$ ). Since in Eqs. (12) and (14),  $\Delta_r$  appears only in even powers, both off-resonant rates  $\ell = 0, 2$  are equally suppressed with respect to the resonant rate  $\ell = 1$ , as highlighted in Tab. 2.

	$\Delta_r^* = 0$	$\Delta_r^* = \pm 3\gamma_e$	$\Delta_r^* = \pm 10\gamma_e$
$\Gamma^{0 \rightarrow 1}(\Delta_r^*)/\gamma_e$	$3.00 \cdot 10^{-4}$	$8.80 \cdot 10^{-6}$	$7.54 \cdot 10^{-7}$
$\Gamma^{1 \rightarrow 0}(\Delta_r^*)/\gamma_e$	$9.00 \cdot 10^{-4}$	$7.14 \cdot 10^{-7}$	$5.64 \cdot 10^{-9}$

**Table 2.** Calculation of the creation [ $\Gamma^{0 \rightarrow 1}(\Delta_r^*)$ ] and destruction [ $\Gamma^{1 \rightarrow 0}(\Delta_r^*)$ ] rates of a Rydberg excitation (in units of  $\gamma_e$ ), from Eqs. (12) and (14), for  $\Delta_r^* = 0$  (resonant rates) and  $\Delta_r^* = \pm 3\gamma_e, \pm 10\gamma_e$  (far-off-resonant rates). Other parameters are:  $\Omega_e = \gamma_e$  and  $\Omega_r = 0.03\gamma_e$ . The difference between resonant and far-off-resonant rates is of several order of magnitudes and increases with  $\Delta_r^*$ .

The choice of  $V = \Delta_r$  as the largest energy scale is motivated by the fact that, in absence of this condition, the strong transition  $|g\rangle \leftrightarrow |e\rangle$  might significantly increase the probability of occurrence of the originally suppressed  $\ell = 0, 2$  processes of excitation (deexcitation) to (from)  $|r\rangle$ . As a consequence of the difference between rates, the relaxation dynamics shows a large separation of timescales (see Sec. 4). These constrained processes are analogous to the ones occurring in Spin Facilitated Models, which we discuss in the following.

### 3. Spin Facilitated Models

Spin Facilitated Models (SFMs) are a class of KCMs that exhibit dynamical heterogeneities and slowing down of relaxation timescales [15]. Even though SFMs can be implemented in a variety of lattice geometries and dimensions, from now on we will limit ourselves to  $1d$ . Here, two classical spin variables,  $n_i = 0, 1$ , are directly associated to an atom being in a *bright* and *dark* period, respectively (see Sec. 2).

Assuming that the system is formed by  $N$  of such spins, let us consider the energy functional of non-interacting spins in an external field,

$$E = K \sum_{i=1}^N n_i, \quad (18)$$

introduced by Fredrickson and Andersen [61, 62]. The model in Eq. (18) does not feature a finite temperature phase transition for a field strength  $K \neq 0$ . The equilibrium concentration of defects reads

$$d_{\text{eq}} = \frac{1}{N} \lim_{t \rightarrow \infty} \sum_{i=1}^N n_i(t) = \frac{1}{1 + e^{\beta K}}, \quad (19)$$

where  $n_i(t)$  is the number of spins at time  $t$  which are in the state  $n_i = 1$ ,  $\beta = 1/(k_B T)$ ,  $k_B$  is the Boltzmann's constant and  $T$  is the equilibrium system temperature. Furthermore, for every  $K > 0$ ,  $\lim_{T \rightarrow 0} d_{\text{eq}} = 0$ , in line with the intuition that at low  $T$  the concentration of defects should be small. From now on, we set  $k_B = 1$  and we fix the temperature scale setting  $K = 1$ .

Despite the simple ground-state of Eq. (18), the non-equilibrium dynamics towards it can be non-trivial. In general, the evolution of  $N$  classical spins is described by the following rate equation for the probabilities  $p(\mathbf{n}, t)$  of being in the many-body spin state specified by the vector  $\mathbf{n} = (n_1, \dots, n_i, \dots, n_N)$  at time  $t$ :

$$\frac{\partial p(\mathbf{n}, t)}{\partial t} = \sum_{\mathbf{m} \neq \mathbf{n}} \{ \Gamma(\mathbf{m} \rightarrow \mathbf{n}) p(\mathbf{m}, t) - \Gamma(\mathbf{n} \rightarrow \mathbf{m}) p(\mathbf{n}, t) \}. \quad (20)$$

Here,  $\Gamma(\mathbf{m} \rightarrow \mathbf{n})$  is the rate associated with the transition from  $\mathbf{m}$  to  $\mathbf{n} \neq \mathbf{m}$ . The equilibrium probabilities  $\pi(\mathbf{m}, t)$  satisfy detailed balance  $\Gamma(\mathbf{m} \rightarrow \mathbf{n}) \pi(\mathbf{m}, t) = \Gamma(\mathbf{n} \rightarrow \mathbf{m}) \pi(\mathbf{n}, t)$  with respect to Eq. (18). Under the assumption of (i) *local* spin-flips and (ii) Glauber-like dynamics [63], the transition rate from  $(n_1, \dots, n_i, \dots, n_N)$  to  $(n_1, \dots, 1 - n_i, \dots, n_N)$  at site  $i$ ,  $\Gamma^{n_i \rightarrow 1 - n_i}$ , is equal to  $1/(1 + e^{\beta \Delta E})$ , with  $\Delta E = 1 - 2n_i$  the difference between the energies of the final and initial spin configurations. From Eq. (19) follows that

$$\Gamma^{n_i \rightarrow 1 - n_i} = (1 - d_{\text{eq}}) n_i + d_{\text{eq}} (1 - n_i). \quad (21)$$

Thus, the asymmetry in the ratio of the rates of creation over destruction of a defect

$$\frac{\Gamma^{0 \rightarrow 1}}{\Gamma^{1 \rightarrow 0}} = \frac{d_{\text{eq}}}{1 - d_{\text{eq}}}, \quad (22)$$

fixes the temperature  $T$  at which the system of non-interacting spins thermalizes. (Note that  $\Gamma^{0 \rightarrow 1} \rightarrow \Gamma^{1 \rightarrow 0}$  for  $T \rightarrow \infty$ .)

Up to now, all transitions  $(n_1, \dots, n_i, \dots, n_N) \rightarrow (n_1, \dots, 1 - n_i, \dots, n_N)$  are allowed in the dynamics. The key idea behind SFMs is to introduce some restrictions in the transitions from one configuration to another: a spin flip  $n_i \rightarrow 1 - n_i$  is allowed only if there are enough defects in the neighbourhood that can facilitate it. In the 1-SFM, such

kinetic constraints require that a spin can flip provided *at least* one of its two neighbors is a defect. This facilitation condition transforms Eq. (21) into

$$\Gamma^{n_i \rightarrow 1-n_i} = (n_{i-1} + n_{i+1}) \{(1 - d_{\text{eq}})n_i + d_{\text{eq}}(1 - n_i)\}. \quad (23)$$

The association between rates in Eq. (23) and the many-body rates calculated in Subsec. 2.2 is straightforward:  $n_{i-1} = n_{i+1} = 0$  corresponds to  $\ell = 0$  for which no spin flip at site  $i$  is allowed, while either  $\{n_{i-1} = 1, n_{i+1} = 0\}$  or  $\{n_{i-1} = 0, n_{i+1} = 1\}$  corresponds to  $\ell = 1$  and atom  $i$  is facilitated to flip its spin. The only difference arises in the case of  $n_{i-1} = n_{i+1} = 1$ : while rates in the 1-SFM are doubled with respect to the case  $\{n_{i-1} = 1, n_{i+1} = 0\}$ , for  $\ell = 2$  rates are suppressed as much as for  $\ell = 0$ . This will lead to differences in the dynamics of the two systems which we will discuss in Sec. 4.

## 4. Numerical results

### 4.1. Classical regime

In the limit of strong driving to the intermediate state  $\Omega_e \sim \gamma_e$  with  $\Omega_r \ll \Omega_e^2/\gamma_e$ , the system approaches the classical regime due to the coupling to the strongly dissipative level  $|e\rangle$ . We consider quantum trajectory simulations of Eqs. (1) and (16) with  $\Delta'_{ri} = 0$  and periodic boundary conditions (PBCs). In Fig. 3, the trajectory of the Rydberg populations  $r_\alpha(t)$  [Eq. (8)] of each atom for two different parameter sets are compared. While for  $\Delta_r = V = 0$  [panel (a)], the dynamics of Rydberg excitations is unconstrained and each atom is independent, for  $\Delta_r = V \neq 0$  [panel (b)] clear spatial correlations emerge and the dynamics of Rydberg excitations resembles the dynamics of defects in the 1-SFM [15, 64]. For  $\Delta_r = V \neq 0$ , we find three different species of atoms which we label, in analogy to the language of SFMs, as:

- *defects*, that is atoms in  $|r\rangle$ ;
- *facilitated* atoms, that is atoms in either  $|g\rangle$  or  $|e\rangle$  with one *defect* as nearest-neighbor;
- *non-facilitated* atoms, that is atoms in either  $|g\rangle$  or  $|e\rangle$  with no *defect* as nearest-neighbor.

As an example, a diffusion process of a *defect* in our model [blue ellipse in Fig. 3(b)] is very similar to the diffusion of a defect in the 1-SFM:

(i) A *defect* facilitates the (Rydberg-)excitation of a *facilitated* atom [red ellipse in Fig. 3(b)], with rate  $\Gamma^{0 \rightarrow 1}(0)$ ; (ii) these two nearest-neighbour *defects* facilitate each other to relax to  $|g\rangle$ , with a larger rate  $\Gamma^{1 \rightarrow 0}(0)$  [see Tab. 2]; (iii) if the original *defect* relaxes first, we have an effective diffusion process of the original *defect* of one site, otherwise the starting configuration is restored. We point out that in the limit  $T \ll 1$  (or equivalently  $d_{\text{eq}} \ll 1$ ),  $\Gamma^{0 \rightarrow 1}(0)/\Gamma^{1 \rightarrow 0}(0) \sim d_{\text{eq}} \sim e^{-\beta}$  from Eq. (22) and the diffusion constant of the process is  $\sim d_{\text{eq}}/2$  [15]. The factor 1/2 takes into account the case in which the newly created *defect* relaxes before the original *defect*. Note that, within the

choice of parameters of Fig. 3,  $\Gamma^{0 \rightarrow 1}(0)/\Gamma^{1 \rightarrow 0}(0) = 1/3$ , but the diffusion constant does not have an analogously simple analytical expression.

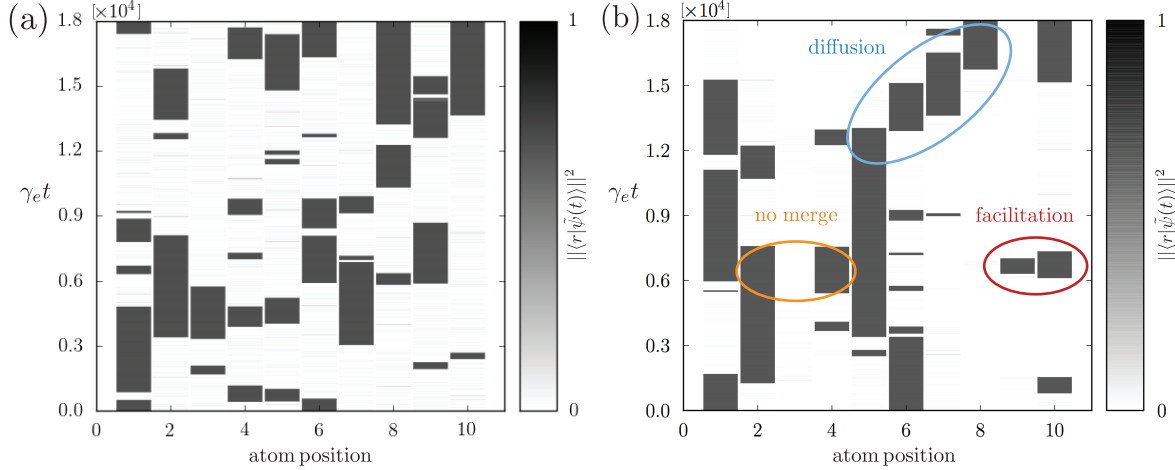


**Figure 3.** Comparison of a typical trajectory of Rydberg excitations in the unconstrained case  $\Delta_r = V = 0$  [panel (a)] and facilitated case  $\Delta_r = V = 10\gamma_e$  [panel (b)]. Other parameters are:  $N = 10, \Omega_e = \gamma_e, \Omega_r = 0.03\gamma_e$ . The initial condition is two Rydberg excitations in  $i = 1$  and  $i = 6$ , while all other atoms are in  $|g\rangle$ . Processes of facilitation and diffusion (typical of 1-SFMs) and avoided merging (not present in 1-SFMs) are highlighted in panel (b).

In the following, we study the relaxation dynamics of the aforementioned three different species. Results averaged over  $N_{\text{traj}}$  different trajectories are depicted in Fig. 4. All trajectories have the same initial state, that is two *defect* far apart from each other. *Facilitated* atoms (red lines) show similar dynamics with respect to resonantly driven single atoms, due to the anti-blockade condition which acts as a facilitating term in the 1-SFM [cfr. Eq. (23)]. The inset of Fig. 4 shows that, in proximity of  $t = 0$ , the profiles of *facilitated* atoms is very well approximated by the resonant [ $\Delta_r = 0$ ]  $\rho_{rr}(t)$ , the associated transition rate being  $\Gamma^{0 \rightarrow 1}(0)$  [Eq. (15)].

The dynamics of *defects* and *non-facilitated* atoms is slowed down with respect to the one of *facilitated* atoms. At  $t = 0$ , the weak transition  $|g\rangle \leftrightarrow |r\rangle$  of a *defect* (blue lines) is far-off-resonant and the related rate  $\Gamma^{1 \rightarrow 0}(\Delta_r)$  [Eq. (12)] is orders of magnitude suppressed with respect to  $\Gamma^{1 \rightarrow 0}(0)$  [cfr. Tab. 2]. Similarly, *non-facilitated* atoms (black lines), in order to be excited to the Rydberg state, have to wait for one of their two neighbors to be Rydberg-excited too. The inset of Fig. 4 shows that, in proximity of  $t = 0$ , the profiles of *non-facilitated* atoms agree with the far-off resonant [ $\Delta_r \neq 0$ ]  $\rho_{rr}(t)$ , the associated transition rate being  $\Gamma^{0 \rightarrow 1}(\Delta_r)$  [Eq. (14)].

Note that, while for  $N = 10$  and assuming PBCs, *facilitated* atoms are neighbors of both *defects* and *non-facilitated* atoms, for larger  $N$  we predict the existence of *non-facilitated* atoms with profiles of  $R_i(t)$  even slower than the ones in Fig. 4. This can be regarded as a form of hierarchical relaxation [20] typical of glasses, in that the more distant the *non-facilitated* atom is from a *defect* at  $t = 0$ , the more slowed-down  $R_i(t)$

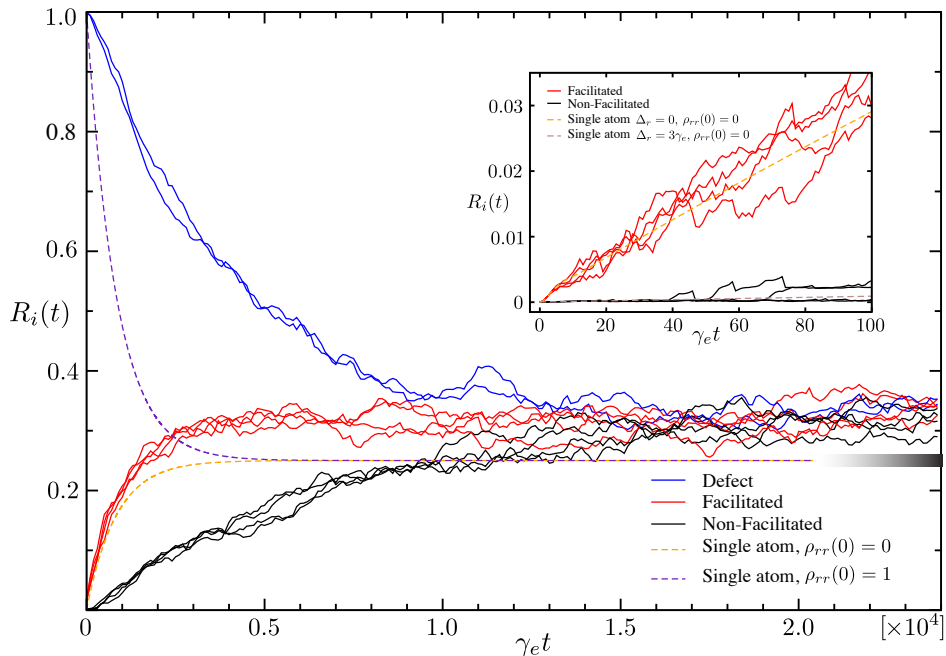


**Figure 4.** Evolution of the trajectory averaged Rydberg population  $R_i(t)$  for  $N_{\text{traj}} = 500$  in a chain of  $N = 10$  sites. Parameters are:  $\Omega_e = \gamma_e$ ,  $\Omega_r = 0.03\gamma_e$ ,  $\Delta_r = V = 3\gamma_e$ ,  $\Delta'_r = 0$ . The initial state is: *defects* (blue lines) at  $i = 1$  and  $i = 6$ ; *facilitated* atoms (red lines) at  $i = 2, 5, 7, 10$  and *non-facilitated* atoms (black lines) at  $i = 3, 4, 8, 9$ . Exact master equation evolution of the single atom Rydberg population  $\rho_{rr}(t)$  are shown for the initial states  $\rho_{rr}(0) = 0$  (orange dotted line) and  $\rho_{rr}(0) = 1$  (indigo dotted line). The result  $r > d_{\text{eq}}$ , suggests that our system lacks of a true thermalisation to the ground-state of the 1-SFM (see main text). The shaded thick black line is the value of  $d_{\text{eq}} = 0.25$  according to Eq. (27). Inset: Resonant (orange dotted line) and off-resonant (light brown dotted line) profiles  $\rho_{rr}(t)$  of a single atom well approximate the short time dynamics of *facilitated* and *non-facilitated* atoms, respectively.

will be.

We now consider the transient concentration of Rydberg excitations

$$r(t) = \frac{1}{N} \sum_{i=1}^N R_i(t). \quad (24)$$

The dynamics of  $r(t)$  for different  $N$  and  $V$ , starting with the same initial state is depicted in Fig. 5. After an initial transient relaxation,  $r(t)$  reaches a steady state with a constant value  $r \equiv \lim_{t \rightarrow \infty} r(t)$ , except for the case of the largest system size  $N = 10$  and smaller interaction strength  $V = 3\gamma_e$ , where it increases with a small but clear trend in the long time limit. We determine the origin of this anomalous slow growth of  $r(t)$  in the excess number of *defects* created from *non-facilitated* atoms within  $\ell = 0$  suppressed (...000...  $\rightarrow$  ...010...) processes, which give a negative temperature contribution in the SFM language [compare Eq. (19) with Eq. (22)]. The reason why all reverse  $\ell = 0$  processes of destruction of isolated Rydberg excitations (...010...  $\rightarrow$  ...000...), which would tend to diminish  $r(t)$ , are not relevant is because of the asymmetry between

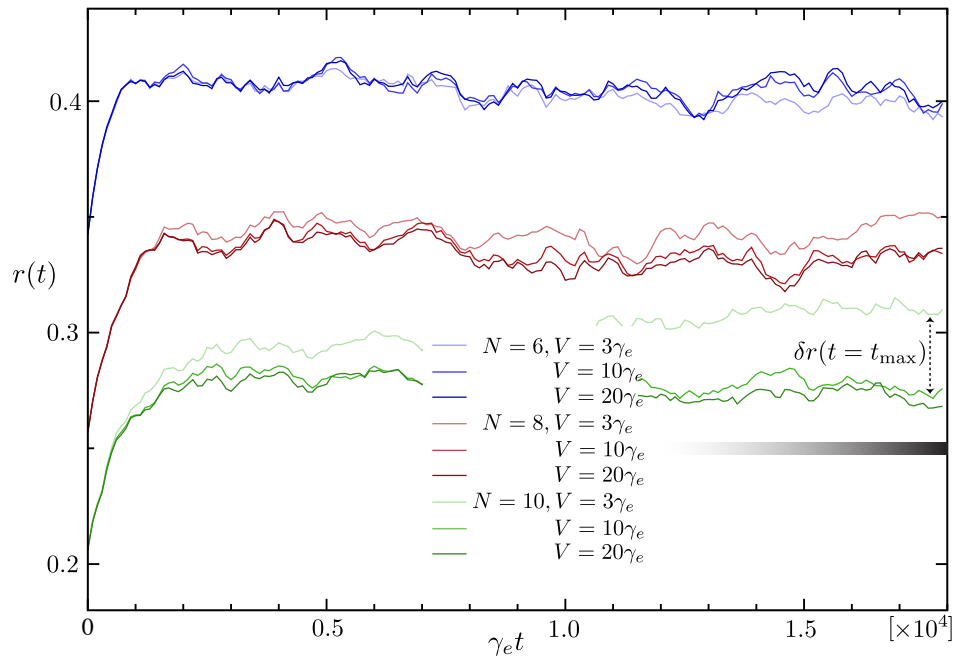


**Figure 5.** Evolution of the concentration of Rydberg excitations  $r(t)$  for  $N = (6, 8, 10)$ , at different interaction strengths,  $V = (3, 10, 20)\gamma_e$ . Parameters are the same as in Fig. 4 and the initial state is, for all plots, two *defects* as far as possible from each other: assuming PBCs, for  $N = 6$  the initial largest distance is 3, for  $N = 8$  is 4, and for  $N = 10$  is 5. The length of the dotted line agrees with  $\delta r(t = t_{\max})$  of the main text.

the off-resonant rates  $\Gamma^{0 \rightarrow 1}(\Delta_r) > \Gamma^{1 \rightarrow 0}(\Delta_r)$  [see Tab. 2], which increases with  $\Delta_r$ , as depicted in the inset of Fig. 10. The difference  $\delta r(t)$  between the excess in the concentration of Rydberg excitations at time  $t$  and the steady state value  $r$  due to (...000...  $\rightarrow$  ...010...) processes is

$$\delta r(t) = \frac{N_{\text{nf}} \cdot \Gamma^{0 \rightarrow 1}(\Delta_r) \cdot t}{N}, \quad (25)$$

where  $N_{\text{nf}}$  is the number of *non-facilitated* atoms at  $t = 0$ , which we assume constant in time. In our case, at the final time of the trajectory  $t_{\max}$ ,  $\delta r(t = t_{\max}) \sim 0.06$ , which well agrees with numerical results plotted in Fig. 5, within statistical errors due to finite  $N_{\text{traj}}$  simulated. Contrarily, the difference  $-\delta r'(t)$  between the lack in the concentration of Rydberg excitations at time  $t$  and the steady state value  $r$  due to (...010...  $\rightarrow$  ...000...) processes is

$$-\delta r'(t) = \frac{N_{\text{d}} \cdot \Gamma^{1 \rightarrow 0}(\Delta_r) \cdot t}{N}, \quad (26)$$

where  $N_{\text{d}}$  is the number of isolated *defects* at  $t = 0$ , which we assume constant in time. Within our parameters,  $\delta r'(t = t_{\max}) \sim 0.003$ , which is negligible with respect to both finite  $N_{\text{traj}}$  errors and  $\delta r(t)$ . Tuning  $\Delta_r = V$  to sufficiently large values, allows one to inhibit both  $l = 0$  off-resonant processes reducing  $\Gamma^{0 \rightarrow 1}(\Delta_r)$  and  $\Gamma^{1 \rightarrow 0}(\Delta_r)$  [Eqs. (25)

and (26)]: e.g., for  $\Delta_r = V = (10, 20)\gamma_e$ , the slow growth of  $r(t)$  is suppressed also for  $N = 10$  (see green lines in Fig. 5).

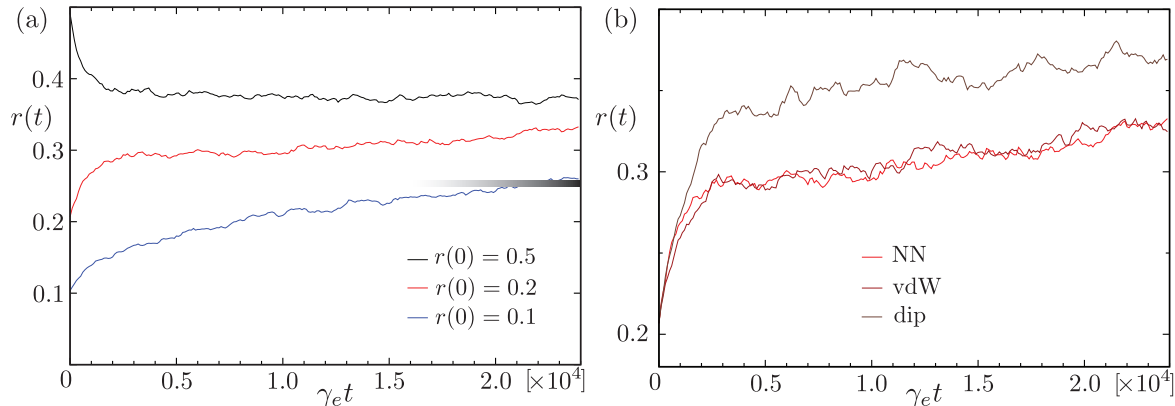


**Figure 6.** Panel (a): Evolution of the concentration of Rydberg excitations  $r(t)$  for different initial states  $r(0)$ . Parameters are the same as in Fig. 4. The initial configurations, assuming PBCs, are:  $r(0) = 0.5$  (black line), with *defects* at  $i = 1, 2, 5, 7, 8$ ;  $r(0) = 0.2$  (red line), with *defects* at  $i = 1$  and  $i = 5$ ;  $r(0) = 0.1$  (blue line), one *defect* (due to PBCs, its position is irrelevant). Panel (b): Evolution of the concentration of Rydberg excitations for the initial state  $r(0) = 0.2$  of panel (a) for nearest-neighbour (NN), van der-Waals (vdW) and dipolar (dip) potentials. In the last two cases, interactions have been truncated to third-nearest neighbour, which we verified to be a good approximation.

All far-off-resonant  $\ell = 2$  processes in Fig. 5 of merging ( $\dots 101\dots \rightarrow \dots 111\dots$ ) and splitting ( $\dots 111\dots \rightarrow \dots 101\dots$ ) of Rydberg excitations are inhibited by the initial concentration  $r(0)$  and configuration of Rydberg excitations: in fact, for e.g. the initial state of two far *defects*, the probability of merging and splitting processes to occur in a trajectory is very small, even if, as highlighted in Fig. 3, at relatively large times avoided merging processes can appear.

In the presence of both merging and splitting processes, which are allowed in the 1-SFM, the system thermalizes to the equilibrium temperature  $T$  determined by the ground-state concentration of Rydberg excitations

$$d_{\text{eq}} = \frac{\gamma_e^2}{2(\gamma_e^2 + \Omega_e^2)}, \quad (27)$$

[from Eqs. (15) and (22)]. It can be verified that  $d_{\text{eq}}$ , in the limit  $\Omega_r \ll \Omega_e, \gamma_e$ , is well approximated by the single-atom steady state Rydberg population  $\rho_{rr}(t \rightarrow \infty)$  calculated in Appendix C. This confirms that the equilibrium ground-state of the 1-SFM is trivial, despite its spatially correlated transient dynamics.

Simulations of our model, depicted in Fig. 5, show that  $r > d_{\text{eq}}$ , contrarily to the result expected from the 1-SFM,  $r = d_{\text{eq}}$ . The reason is in the avoided merging and splitting processes of *defects*, for times smaller than timescales at which off-resonant  $l = 0, 2$  processes become activated: our system does not thermalize to  $T$ , but to a

different steady state (see plateaus in Fig. 5). Nevertheless, with increasing  $N$  the value of  $r$  decreases, as trajectories in which merging processes might occur become much less probable, and the dynamics of our system approaches the one of the 1-SFM. Finally, in Fig. 6(a), we show that the result  $r > d_{\text{eq}}$  has some generality, in that it does not depend on the particular initial state chosen in Fig. 5.

#### 4.2. Quantum Regime

In the limit of vanishing driving of the  $|g\rangle \leftrightarrow |e\rangle$  transition,  $\Omega_e \ll \gamma_e, \Omega_r$ , the dynamics, up to times  $t \ll \gamma_e/\Omega_e^2$ , is dominated by  $|g\rangle \leftrightarrow |r\rangle$  coherences. Starting from the fully coherent limit  $\Omega_e = 0$ , one can study, increasing  $\Omega_e$ , the crossover to the classical rate equation limit of Subsec. 4.1, i.e.  $\Omega_e \sim \gamma_e$  with  $\Omega_r \ll \Omega_e^2/\gamma_e$ .

In the case of  $\Omega_e = 0$ , the system Hamiltonian is that of  $N$  interacting two-level atoms

$$H_{\text{tl}} = \sum_{i=1}^N \left\{ \frac{\Omega_r}{2} (|g\rangle\langle r|_i + \text{H.c.}) - \Delta_r |r\rangle\langle r|_i \right\} + V \sum_{i=1}^{N-1} \left\{ |r\rangle\langle r|_i \otimes |r\rangle\langle r|_{i+1} \right\}. \quad (28)$$

Assuming, as in in Subsec. 4.1,  $\Omega_r \ll \Delta_r$  and  $V = \Delta_r$ , at times  $t \ll \Delta_r/\Omega_r^2$ , the system explores only a subspace of the full Hilbert space of  $H_{\text{tl}}$ . This subspace, illustrated in Fig. 7 for  $N = 3, 4$ , is univocally defined by the initial state.

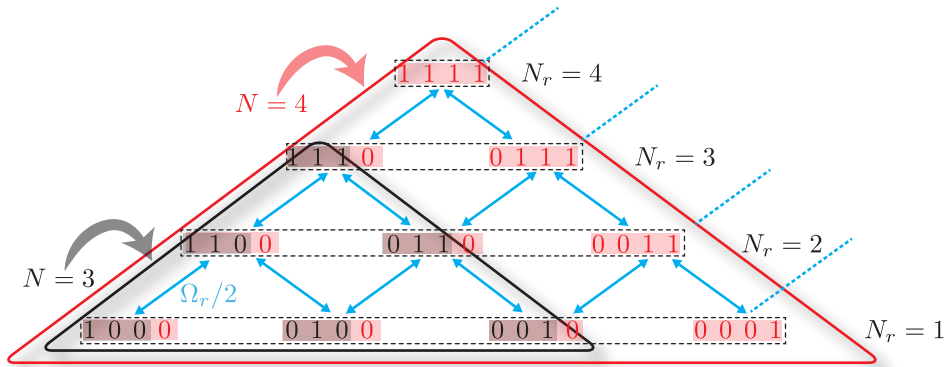


**Figure 7.** Scheme of the effective dynamics governed by the Hamiltonian in Eq. (28) with open boundary conditions (OBCs) for  $t \ll \Delta_r/\Omega_r^2$ , given an initial state with energy  $-V$  (see main text). The binary values 0 and 1 represent here an atom in  $|g\rangle$  and  $|r\rangle$ , respectively. All allowed system configurations are coupled with the single atom Rabi frequency  $\Omega_r/2$  (blue arrows). The black (red) triangle refers to the case with  $N = 3$  ( $N = 4$ ) atoms. In each row, the total number of Rydberg excitations  $N_r$  is constant, independently of  $N$ . Increasing the number of atoms from  $N = 3$  to  $N = 4$ , results in adding a diagonal group of  $N = 4$  new states (highlighted in shaded red) and adding a 0 in the rightmost site of all  $N = 3$  states (highlighted in shaded black). This scheme can be generalized to an arbitrary  $N$ .

The dynamics governed by  $H_{\text{tl}}$  and limited to the aforementioned subspace can be understood from an effective cluster model which we derive in the following. Consider

the example of  $N = 3$  atoms. In this case the Hamiltonian in Eq. (28) is represented, in the basis  $\{|ggg\rangle, |rgr\rangle, |ggr\rangle, |grg\rangle, |grr\rangle, |rgg\rangle, |rrg\rangle, |rrr\rangle\}$ , by the matrix

$$\mathcal{H}_{\text{cl}}^{N=3} = \begin{pmatrix} 0 & 0 & \frac{\Omega_r}{2} & \frac{\Omega_r}{2} & 0 & \frac{\Omega_r}{2} & 0 & 0 \\ 0 & -2V & \frac{\Omega_r}{2} & 0 & 0 & \frac{\Omega_r}{2} & 0 & \frac{\Omega_r}{2} \\ \frac{\Omega_r}{2} & \frac{\Omega_r}{2} & -V & 0 & \frac{\Omega_r}{2} & 0 & 0 & 0 \\ \frac{\Omega_r}{2} & 0 & 0 & -V & \frac{\Omega_r}{2} & 0 & \frac{\Omega_r}{2} & 0 \\ 0 & 0 & \frac{\Omega_r}{2} & \frac{\Omega_r}{2} & -V & 0 & 0 & \frac{\Omega_r}{2} \\ \frac{\Omega_r}{2} & \frac{\Omega_r}{2} & 0 & 0 & 0 & -V & \frac{\Omega_r}{2} & 0 \\ 0 & 0 & 0 & \frac{\Omega_r}{2} & 0 & \frac{\Omega_r}{2} & -V & \frac{\Omega_r}{2} \\ 0 & \frac{\Omega_r}{2} & 0 & 0 & \frac{\Omega_r}{2} & 0 & \frac{\Omega_r}{2} & -V \end{pmatrix}. \quad (29)$$

If the initial state has energy  $-V$ , i.e. if we start from one of  $|rgr\rangle, |ggr\rangle, |grg\rangle, |grr\rangle, |rgg\rangle$ , or  $|rrg\rangle$  (or any linear combination of them), the system dynamics, at times  $t \ll \Delta_r/\Omega_r^2$ , will be limited in the subspace defined by the matrix  $\tilde{\mathcal{H}}_{\text{cl}}^{N=3}$  enclosed by the dotted lines in the down-right corner of  $\mathcal{H}_{\text{cl}}^{N=3}$  in Eq. (29). Within this choice of the initial state, the subspace is characterized by the presence of one cluster of Rydberg excitations with varying size (that is, the number of Rydberg excitations next to each other  $N_r$  changes during the dynamics). Here, a cluster is defined as a group of contiguous Rydberg excitations without atoms in  $|g\rangle$  in between them. We point out that, at  $t \gtrsim \Delta_r/\Omega_r^2$ , second (and higher) order perturbative processes in the small parameter  $\Omega_r/\Delta_r \ll 1$  will drive the dynamics outside the subspace. This discussion can be extended also for a general  $N$ . Remarkably, the dimension of  $\tilde{\mathcal{H}}_{\text{cl}}^N$  scales as  $N(N+1)/2$  contrarily to the exponential growth,  $2^N$ , of the full matrix  $\mathcal{H}_{\text{cl}}^N$ .

In Fig. 8, we compare, for  $N = 9$ , the evolution of  $r(t)$  governed by  $\mathcal{H}_{\text{cl}}^{N=9}$  (green line) and  $\tilde{\mathcal{H}}_{\text{cl}}^{N=9}$  (red line). We restrict the dynamics of the system in the subspace with energy  $-V$  starting with one Rydberg excitation in the center of the open chain and all the remaining atoms in  $|g\rangle$ . Numerical simulations of the full ( $\mathcal{H}_{\text{cl}}^{N=9}$ ) and effective ( $\tilde{\mathcal{H}}_{\text{cl}}^{N=9}$ ) dynamics are in excellent agreement for  $t \ll \Delta_r/\Omega_r^2$ . In this time window, the peaks of the oscillations of  $r(t)$  have a periodicity  $2\pi/(\Omega_r/2)$ .

Let us now study the general properties of  $\tilde{\mathcal{H}}_{\text{cl}}^N$  in detail. Setting  $\Delta_r = V = 0$  without loss of generality (in the reduced subspace,  $V$  is a constant energy off-set) and considering again the example  $N = 3$ , the eigenvalues  $E_\lambda^{N=3}$  of  $\tilde{\mathcal{H}}_{\text{cl}}^{N=3}$ , written in ascending order, are

$$E_\lambda^{N=3} = \left( -\frac{\sqrt{5}\Omega_r}{2}, -\frac{\Omega_r}{2}, 0, 0, \frac{\Omega_r}{2}, \frac{\sqrt{5}\Omega_r}{2} \right). \quad (30)$$

In Fig. 9, we plot the spectrum of eigenvalues  $E_\lambda^N$  for different  $N$ . Two properties emerge:

(i) Independently of  $N$ , there is always at least one *dark* state, that is an eigenstates of  $\tilde{\mathcal{H}}_{\text{cl}}^N$  with  $E_\lambda^N = 0$ . The total number of *dark* states for  $N \geq 3$  [ $N \geq 2$ ] odd [even] scales as  $(N+1)/2$  [ $N/2$ ]. In the case of  $N = 3$ , there are thus two (non-normalized) *dark* states,

$$|D^{N=3}\rangle = |rrr\rangle - |grg\rangle \quad \text{and} \quad |E^{N=3}\rangle = |rgg\rangle - |grg\rangle + |ggr\rangle. \quad (31)$$

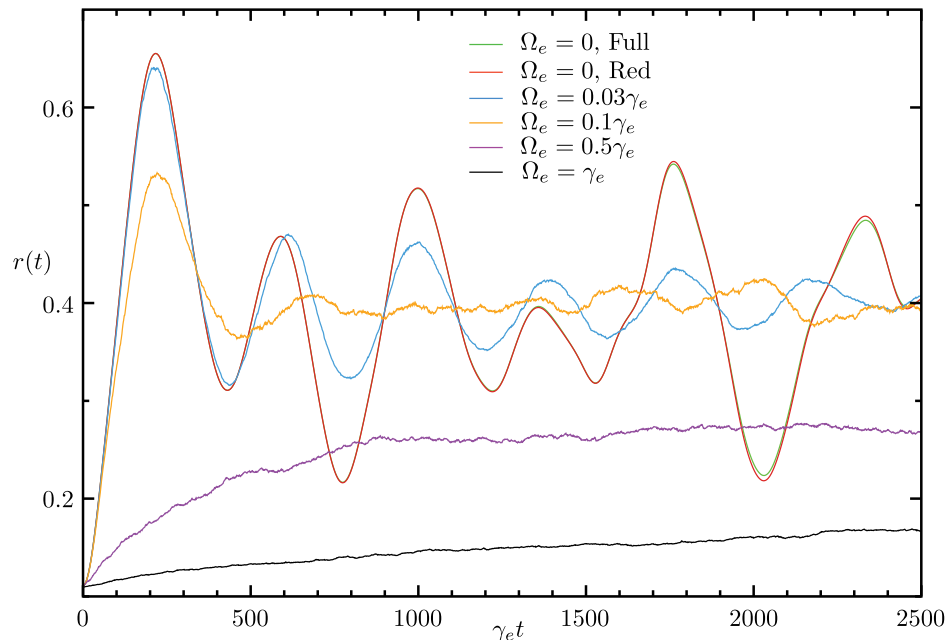


**Figure 8.** Evolution of  $r(t)$  for different  $\Omega_e$ ,  $N = 9$ , and OBCs. Hamiltonian parameters are:  $\Omega_r = 0.03\gamma_e$ ,  $V = \Delta_r = 3\gamma_e$ . The initial state is one *defect* in  $i = 5$ , all other atoms being in  $|g\rangle$ . The green curve plots results of simulations evolving the full Hamiltonian  $\mathcal{H}_{il}^{N=9}$  at  $\Omega_e = 0$ . The red curve reproduces with high accuracy the exact dynamics evolving the reduced matrix  $\tilde{\mathcal{H}}_{il}^{N=9}$  (see main text). For all  $\Omega_e \neq 0$ ,  $N_{\text{traj}} = 500$  trajectories have been simulated and averaged.

Since the number of *dark* states scales linearly with  $N$ , they can also be interpreted as *edge* states: for example,  $|E^{N=3}\rangle$  in Eq. (31) is localized at the lower boundary of the scheme depicted in Fig. 7.  $|E^N\rangle$  exists, in general, for every  $N$ , and it is obtained from the linear combination of all states consisting of only one Rydberg excitation with alternating plus and minus signs, in analogy to Eq. (31).

(ii) The number of eigenvalues scale for  $N \geq 3$  [ $N \geq 2$ ] odd [even] as  $(N^2 - 1)/4$  [ $N^2/4$ ]. The corresponding spectrum, shown in Fig. 9 for different  $N$ , is bounded by  $-2\Omega_r$  and  $2\Omega_r$  for large  $N$ .

This as a consequence of the fact that the coupling between all allowed states of the reduced subspace can be interpreted, in the thermodynamic limit  $N \rightarrow \infty$ , as hopping processes of a single particle in an artificial two-dimensional square lattice. This model is known as the two-dimensional tight-binding model, whose dispersion relation is

$$\varepsilon(\vec{q}) = -2J\{\cos(q_1s) + \cos(q_2s)\}. \quad (32)$$

Here,  $\varepsilon(\vec{q})$  is the energy of the particle at quasi-momentum  $\vec{q}$ ,  $J$  is the hopping amplitude between adjacent lattice sites,  $s$  is the lattice spacing of the Bravais lattice and  $\vec{q} = q_1\vec{b}_1 + q_2\vec{b}_2$ .  $\vec{b}_{1,2} = (2\pi/s^2)\vec{a}_{1,2}$  are the vectors which span the reciprocal lattice of the Bravais lattice generated by  $\vec{a}_1 = s(1, 0)$  and  $\vec{a}_2 = s(0, 1)$  and  $\{(1, 0), (0, 1)\}$  is the standard basis in the Euclidean plane. Furthermore, due to PBCs,  $q_{1,2}s = 2\pi m_{1,2}/N$  and  $m_{1,2} \in [-N/2, N/2]$ . Thus, from Eq. (32),  $\varepsilon(\vec{q})$  has a maximum width of  $8J$ . In our

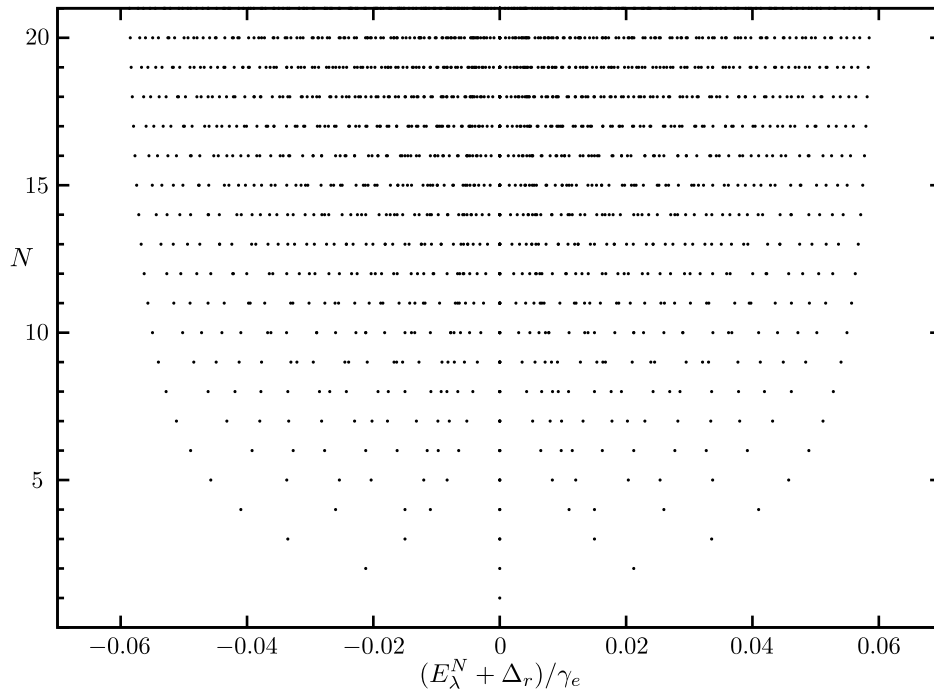


**Figure 9.** Eigenvalues spectrum for  $\Omega_r = 0.03\gamma_e$  and  $\Delta_r = 0$  at different  $N$ . In the thermodynamic limit  $N \rightarrow \infty$ , the spectrum is bounded by  $\pm 2\Omega_r$ , according to the two-dimensional tight binding model dispersion relation [see Eq. (32) and the related discussion in the main text].

case  $J = \Omega_r/2$ , which gives exactly the spectrum width of  $4\Omega_r$  observed in Fig. 9 for large  $N$ . We stress that the mapping to the two-dimensional tight binding model, which reduces a  $d$ -dimensional many-body problem with nearest-neighbour interactions to a  $(d+1)$ -dimensional single particle problem, is exact only in the limit  $N \rightarrow \infty$ , where boundary effects in our model tend to zero, i.e. PBCs hold.

Let us now study the transition from the fully coherent limit to the classical limit switching on and increasing  $\Omega_e$ , while keeping fixed all other parameters. Even for small  $\Omega_e = (0.03, 0.1)\gamma_e$  (blue and orange lines, respectively, in Fig. 8), the system dynamics deviates from the coherent case, since  $\Omega_e \gtrsim \Omega_r$ , and oscillations of  $r(t)$  are damped by dissipative processes due to the coupling to the short-lived intermediate level  $|e\rangle$ . For  $t \gg \gamma_e/\Omega_e^2$ ,  $r(t)$  is driven to its steady state value  $r$ , which is well approximated by  $\rho_{rr}(t \rightarrow \infty)$  [see Appendix C]. Upon further increase of  $\Omega_e$ , the rate equation limit is recovered, in which  $r(t)$  increases slowly with time, oscillations are completely suppressed and, as already discussed in Subsec. 4.1,  $r$  does not coincide with  $\rho_{rr}(t \rightarrow \infty)$ .

### 4.3. External disorder

The external disorder, arising from static spatially-random detunings from  $|r\rangle$ ,  $\Delta'_{ri} \neq 0$  in Eq. (1), considerably changes the dynamics of the relaxation. In the quantum regime,

they are responsible of the many-body localization transition [11, 12, 13, 14]. Here, we focus on the rate equation limit. We randomly choose the values of  $\Delta'_{ri}$  within the interval  $[-A, A]$  according to a uniform distribution. Moreover, we assume  $0 < A \ll \Delta_r$ , in order to avoid accidental local balancing of the homogeneous and random detunings,  $\Delta'_{ri} \sim \Delta_r$ . Quantum trajectories are simulated according to the following procedure: (i) construct  $N_{\text{rnd}}$  different sets of random detunings  $(\Delta'_{r1}, \dots, \Delta'_{ri}, \dots, \Delta'_{rN})$  to be added to the homogeneous detuning  $\Delta_r$ ; (ii) for each random field configuration  $(\Delta'_{r1} + \Delta_r, \dots, \Delta'_{ri} + \Delta_r, \dots, \Delta'_{rN} + \Delta_r)$ , simulate  $N_{\text{traj}}$  stochastically independent quantum trajectories; (iii) average the desired observable over the total number of trajectories  $N_{\text{traj}}N_{\text{rnd}}$ . Note that, for sufficiently large  $N_{\text{rnd}}$ , no extra energy is added to the system, because  $[-A, A]$  is centered around 0.

Fig. 10 shows that increasing  $N_{\text{rnd}}$  (for a sufficiently large  $N_{\text{traj}}$ ), all atoms relax faster toward the steady state with respect to the case of zero random detuning. This tendency can be understood looking at Tab. 3, which summarizes the effect of  $\Delta'_{ri} \neq 0$  on each species.

<i>Facilitated:</i> $\Delta_r^* = 0$		<i>Defect/Non-Fac.:</i> $\Delta_r^* = \Delta_r$		<i>Blocked:</i> $\Delta_r^* = -\Delta_r$	
$0 +  \Delta'_{ri} $	$0 -  \Delta'_{ri} $	$\Delta_r +  \Delta'_{ri} $	$\Delta_r -  \Delta'_{ri} $	$-\Delta_r +  \Delta'_{ri} $	$-\Delta_r -  \Delta'_{ri} $
Speed up	Speed up	Slow down	Speed up	Speed up	Slow down

**Table 3.** Effect of positive (first inner-columns) and negative (second inner-columns) random detunings  $\Delta'_{ri} \in [-A, A]$  (with  $A \ll \Delta_r$ ) on *facilitated* atoms, *defects*, *non-facilitated* atoms and *blocked* atoms. The attribute 'Slow down' ('Speed up') implies that the effective rates  $\Gamma^{n_i \rightarrow 1-n_i}(\Delta_r^* \pm |\Delta'_{ri}|)$  [with  $n_i = 0, 1$ ] are reduced (increased) with respect to zero random detuning rates,  $\Gamma^{n_i \rightarrow 1-n_i}(\Delta_r^*)$ .

Since, as depicted in the inset of Fig. 10, for *facilitated* atoms and within our choice of  $A \ll \Delta_r$ , the rates  $\Gamma^{n_i \rightarrow 1-n_i}(\Delta'_{ri})$  of creation ( $n_i = 0$ ) and destruction ( $n_i = 1$ ) of Rydberg excitations are larger than resonant rates  $\Gamma^{n_i \rightarrow 1-n_i}(0)$  (see plots in the beige area), a *facilitated* atom is sped up by any finite random detuning, independently from its sign. Contrarily, the relaxation of *defects/non-facilitated* atoms (shaded green area) and *blocked* atoms (shaded blue area) is either slowed down or sped up, depending on the sign of  $\Delta'_{ri}$ . Furthermore, considering the same  $\Delta'_{ri}$ , *blocked* atoms ( $\ell = 2$ , see Subsec. 2.2), which are absent at  $t = 0$  and behave exactly like *defects/non-facilitated* atoms for  $\Delta'_{ri} = 0$  [cfr. Eqs. (12) and (14)], are affected in the opposite way with respect to *defects/non-facilitated* atoms. For example, if  $\Delta'_{ri} > 0$ , *defects/non-facilitated* atoms are slowed down, whereas *blocked* atoms are sped up (viceversa in the case of  $\Delta'_{ri} < 0$ ).

In each trajectory with a given random field configuration, we can thus determine, at every time  $t$ , whether the instantaneous relaxation rate at a certain site is sped up or slowed down with respect to the zero random field case. The result of an *averaged* (over trajectories) faster relaxation at all sites can be qualitatively understood from the statistical win of the attribute 'Speed up' with respect to the attribute 'Slow down' in Tab. 3, approximating the number of species to be constant in time and equal to their corresponding values at  $t = 0$ . For the initial state in Fig. 10 of two far *defects* we have:

$N_d = 2$ ,  $N_{nf} = 4$ ,  $N_f = 4$  and  $N_b = 0$  where  $N_f$  and  $N_b$  label the number of *facilitated* and *blocked* atoms, respectively, and  $N = N_d + N_{nf} + N_f + N_b = 10$ . We estimated that 'Speed up' has, on average, an outcome probability of 7/10, contrarily to 3/10 for 'Slow down'. This is a consequence of: (i) the choice of  $A$  and  $\Delta_r$ , for which all  $N_f = 4$  *facilitated* atoms are sped up by any finite  $\Delta'_{ri}$ , leading to a 4/10 outcome probability of 'Speed up' (ii) the fact that *defects/non-facilitated* atoms can be either slowed down or sped up, with equal probability if  $N_{rnd}$  is sufficiently large, as it is the case in Fig. 10, in which plots with different  $N_{rnd}$  overlap. Since  $N_d + N_{nf} = 6$ , we expect, on average, equal probability outcomes of 3/10 for both 'Speed up' and 'Slow down'. Adding the results, we get the aforementioned probability outcomes of 7/10 and 3/10 for 'Speed up' and 'Slow down', respectively.

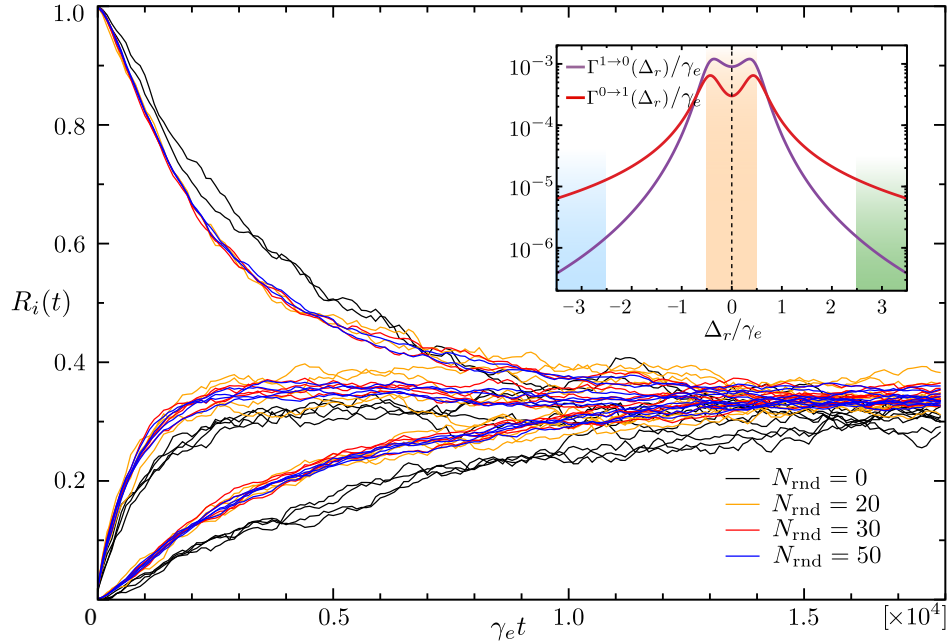


**Figure 10.** Evolution of the trajectory averaged Rydberg population  $R_i(t)$  for different finite random detunings from the Rydberg state,  $\Delta'_{ri} \neq 0$ . The initial configuration and parameters are the same as in Fig. 4 and  $A = 0.5\gamma_e$  (see main text). Different colors refer to different numbers of random detuning configurations  $N_{rnd}$ , for a fixed number of trajectories simulated in each random configuration,  $N_{traj} = 100$ . Inset: Semi-log plot of single particle rates  $\Gamma^{n_i \rightarrow 1-n_i}(\Delta_r)$  [with  $n_i = 0, 1$ ] from Eqs. (12) and (14) as a function of  $\Delta_r$ . The shaded areas delimit the intervals in which the total detuning  $\Delta_r^* \pm |\Delta'_{ri}|$  ranges for *facilitated* atoms (beige), *defects/non-facilitated* atoms (green) and *blocked* atoms (blue).

As a consequence, the overall dynamics towards the steady state is faster in the case of small spatially random detunings with respect to the case of no random detunings. For large random detunings,  $\Delta'_{ri} \in [-A, A]$  with  $A \sim \Delta_r$ , the dynamics is instead slowed down, as *facilitated* atoms have a much higher probability of becoming *non-facilitated*, consistently reducing the probability outcome of 'Speed up' with respect to the case  $A \ll \Delta_r$ .

## 5. Experimental considerations

In the following, we discuss and validate the various assumptions made in Secs. 2 and 4. These are: (i) neglecting the decay from the Rydberg state during the relevant experimental timescales, (ii) truncating long-range van der Waals or dipolar interactions to nearest-neighbor interactions, (iii) assuming atoms in ground- and Rydberg states to be trapped simultaneously in the same optical lattice, and (iv) neglecting heating due to photons emitted from the  $|g\rangle \leftrightarrow |e\rangle$  transition.

(i) The lifetime of Rydberg states is determined by both radiative decay (spontaneous emission) to lower-lying electronic energy levels and blackbody radiation which induces transitions to higher- and lower-lying neighbouring Rydberg states [23, 24]. While for low-lying electronic levels spontaneous decay to the ground-state dominates, for Rydberg states the interaction with thermally occupied infrared photons, which is the main contribution in the overall lifetime, leads to strong mechanical effects [65]. In general, (alkali-metal) Rydberg states have, compared to low-lying excited states, exceedingly long lifetimes  $\propto n^3$  ( $\propto n^5$ ) for low (high) angular momentum states. For  $n \simeq 80$ , these can be of the order of hundreds of  $\mu\text{s}$  [66]. In our setup, the rate of decay from the Rydberg state  $\gamma_r$  can be neglected when

$$\gamma_r \ll \frac{\Omega_e^2 \Omega_r^2 \gamma_e}{4\Delta_r^2 \gamma_e^2 + (\Omega_e^2 - 4\Delta_r^2)^2} \quad (33)$$

holds [60], implying that stimulated emission processes from  $|r\rangle$  have to be much larger than spontaneous ones, which is typically the case for Rydberg states with large enough principal quantum numbers  $n$  and  $\Delta_r = 0$ . For  $\Delta_r \neq 0$ , nonetheless, care has to be taken since, contrarily to the case of the general requirement for well-defined quantum jumps to occur [60]

$$\Omega_r^2 \ll \frac{4\Delta_r^2 \gamma_e^2 + (\Omega_e^2 - 4\Delta_r^2)^2}{\gamma_e^2 + 4\Delta_r^2}, \quad (34)$$

the condition in Eq. (33) becomes *stricter* with respect to the resonant case  $\Delta_r = 0$ .

(ii) In Fig. 6(b) we check, for a certain initial state and no random detunings, the reliability of the approximation of truncating Rydberg interactions to nearest-neighbour. While for van der Waals potentials there is no significant quantitative disagreement, dipolar interactions result to be detrimental, despite the qualitative slow growth of the number of Rydberg excitations is recovered in the long time limit. Nevertheless, Rydberg atoms at distances of a few  $\mu\text{m}$ , typical of large spacing optical lattices [46, 47, 48, 49, 50, 51], are known to interact with van der Waals potentials [23], and our approximation is thus not only qualitatively but also quantitatively justified.

(iii) It is important, in our setup, that atoms are trapped in the same optical lattice during both *bright* and *dark* periods. While ground-state atoms can be trapped using different state-of-the-art techniques, it has been suggested to optically trap Rydberg atoms via ponderomotive potentials from spatially modulated light fields [67] or in dc-electric or magnetic fields [68]. In general, electronic ground-states and Rydberg states will experience different optical trapping potentials due to their different polarizabilities.

A promising route to trap ground-state atoms and Rydberg-atoms in the same lattice is also to use alkaline-earth atoms as suggested in Ref. [69].

(iv) Heating due to photons emitted from the strong transition can be considerably reduced adding a finite detuning from  $|e\rangle$ ,  $\Delta_e \neq 0$ , in order to Doppler-cool atoms with the same fluorescence laser. Results of quantum trajectory simulations (not shown) indicate that the typical slowed relaxation of atoms is qualitatively unaltered, although larger trajectory times with respect to the case  $\Delta_e = 0$  are needed in order to observe the convergence of  $r(t)$  to its steady state value  $r$ .

## 6. Conclusions

We have shown that the non-equilibrium dynamics of Rydberg excitations in three-level atoms can be tuned from the classical to the quantum regime with the laser driving to a short-lived intermediate excited state. The anti-blockade condition, where the nearest-neighbor interaction among Rydberg levels equals the single atom laser detuning from the Rydberg state, implements a form of kinetic constraint. This phenomenon resembles the assisted processes of creation and destruction of defects in the One-Spin Facilitated Model. The absence of merging processes in our system prevents the thermalization to the ground-state of the One-Spin Facilitated Model, despite the concentration of Rydberg excitations can be, in the long time limit, stabilized to some steady state value for sufficiently large interactions and detunings from the Rydberg state. In the intermediate regime of interactions, we observed instead a (tuneable) slow increase of the concentration of Rydberg excitations, caused by the appearance of processes which are not present in the One-Spin Facilitated Model. In this regime, an additional slow relaxation timescale emerges.

In the coherent limit, the dynamics of the resulting interacting two-level system is limited to a subspace of the Hilbert space. This subspace is determined by the choice of the initial state, whose number of clusters of Rydberg excitations is conserved. However, the size of these clusters changes during the evolution. We derived an effective reduced Hamiltonian and verified excellent agreement with simulations of the exact dynamics of the full Hamiltonian.

Finally, we have shown that, in the rate equation limit, the competition of the internal disorder of glasses with an externally imposed disorder can result in the slowing down but also in the speeding up of the overall relaxation towards the steady state. The presented setup allows for the investigation of the quantum dynamics of Spin Facilitated Models in the presence of random fields. As an outlook, we plan to study the dynamics of the coherent cluster model in the spirit of many-body localization.

## Acknowledgments

We thank P. Zoller for initial discussions which stimulated this work. We further acknowledge M. Fleischauer, J. P. Garrahan, I. Lesanovski, B. Olmos, M. Dalmonte, M.

Heyl and H. Pichler. Numerical simulations were performed using QuTip libraries [70]. This work is supported by the Austrian Science Fund (FWF): P-25454, the European Research Council (ERC) Synergy Grant UQUAM, the SFB FOQUS of the Austrian Science Fund and by the Austrian Ministry of Science BMWF as part of the UniInfrastrukturprogramm of the Focal Point Scientific Computing at the University of Innsbruck. M.M. acknowledges the EU Marie-Curie Program ITN COHERENCE FP7-PEOPLE-2010-ITN-265031 for financial support.

## Appendix A. Brillouin-Wigner perturbation theory calculation of eigenvalues and eigenvectors of $H_{\text{eff}}$

Here we summarize the Brillouin-Wigner perturbation theory calculation of the eigenvalues  $\lambda_n$  and eigenvectors  $|u\rangle_n$  of  $H_{\text{eff}}$  in Eq. (4) of the main text, which can be represented, in the  $\{|g\rangle, |e\rangle, |r\rangle\}$  basis, as

$$H_{\text{eff}} = \begin{pmatrix} 0 & \frac{\Omega_e}{2} & \frac{\Omega_r}{2} \\ \frac{\Omega_e}{2} & -i\frac{\gamma_e}{2} & 0 \\ \frac{\Omega_r}{2} & 0 & -\Delta_r \end{pmatrix}. \quad (\text{A.1})$$

Here, we have considered the more general case of a finite laser detuning  $\Delta_r \neq 0$  with respect to  $|r\rangle$ . Assuming  $\Omega_r \ll \Omega_e, \gamma_e, \Delta_r$ , one can split Eq. (A.1) in

$$H_0 = \begin{pmatrix} 0 & \frac{\Omega_e}{2} & 0 \\ \frac{\Omega_e}{2} & -i\frac{\gamma_e}{2} & 0 \\ 0 & 0 & -\Delta_r \end{pmatrix} \quad \text{and} \quad H_1 = \begin{pmatrix} 0 & 0 & \frac{\Omega_r}{2} \\ 0 & 0 & 0 \\ \frac{\Omega_r}{2} & 0 & 0 \end{pmatrix}, \quad (\text{A.2})$$

such that  $H_{\text{eff}} = H_0 + H_1$ , where  $H_0$  is the unperturbed Hamiltonian and  $H_1$  is the perturbation.

We now introduce a unitary transformation  $U = e^{\frac{1}{2} \arctan \left\{ \frac{2i\Omega_e}{\gamma_e} (|e\rangle\langle g| - |g\rangle\langle e|) \right\}}$  which diagonalizes  $H_0$ , such that

$$\tilde{H}_0 = UH_0U^\dagger = \begin{pmatrix} E_m & 0 & 0 \\ 0 & E_p & 0 \\ 0 & 0 & -\Delta_r \end{pmatrix}, \quad (\text{A.3})$$

where  $U^\dagger$  is the Hermitian conjugate of  $U$ ,  $E_m = \frac{i}{4} \left( -\gamma_e + \sqrt{\gamma_e^2 - 4\Omega_e^2} \right)$  and  $E_p = -\frac{i}{4} \left( \gamma_e + \sqrt{\gamma_e^2 - 4\Omega_e^2} \right)$ .

Applying the same transformation on  $H_1$ ,  $\tilde{H}_1 = UH_1U^\dagger$ , we get

$$\tilde{H}_1 = \begin{pmatrix} 0 & 0 & \frac{\Omega_c}{2} \\ 0 & 0 & i\frac{\Omega_s}{2} \\ \frac{\Omega_c}{2} & i\frac{\Omega_s}{2} & 0 \end{pmatrix}, \quad (\text{A.4})$$

where  $\Omega_c = \Omega_r \cosh \{\frac{1}{2} \operatorname{arctanh} \frac{2\Omega_e}{\gamma_e}\}$  and  $\Omega_s = \Omega_r \sinh \{\frac{1}{2} \operatorname{arctanh} \frac{2\Omega_e}{\gamma_e}\}$ . The unitary transformation  $U$  defines a change of basis from  $\{|g\rangle, |e\rangle, |r\rangle\}$  to, say,  $\{|-\rangle, |+\rangle, |r\rangle\}$

$$\begin{cases} |-\rangle = \frac{\Omega_c}{\Omega_r} |g\rangle - i \frac{\Omega_s}{\Omega_r} |e\rangle \\ |+\rangle = i \frac{\Omega_s}{\Omega_r} |g\rangle + \frac{\Omega_c}{\Omega_r} |e\rangle \\ |r\rangle = |r\rangle. \end{cases} \quad (\text{A.5})$$

We now define two operators  $\mathcal{P}$  and  $\mathcal{Q}$  which project onto  $|r\rangle$  and its complementary subspace, respectively. Due to the fact that the transformation generated by  $U$  does not affect the  $|r\rangle$  subspace [see Eq. (A.5)],  $\mathcal{P}$  has the same matrix form in either the  $\{|g\rangle, |e\rangle, |r\rangle\}$  or the  $\{|-\rangle, |+\rangle, |r\rangle\}$  basis

$$\mathcal{P} = \begin{pmatrix} 0 & 0 & 0 \\ 0 & 0 & 0 \\ 0 & 0 & 1 \end{pmatrix}, \quad (\text{A.6})$$

while  $\mathcal{Q}$  can be easily obtained from the orthogonality property of projectors, i.e.  $\mathcal{P} + \mathcal{Q} = \mathbf{1}$ , where  $\mathbf{1}$  is the identity operator.

The first- ( $E_1$ ) and second-order ( $E_2$ ) corrections to  $E_0 = [\mathcal{P}H_0\mathcal{P}]_{3,3} = [\mathcal{P}\tilde{H}_0\mathcal{P}]_{3,3} = -\Delta_r$  of the transformed unperturbed Hamiltonian  $\tilde{H}_0$  are given by

$$E_1 = [\mathcal{P}H_1\mathcal{P}]_{3,3} = [\mathcal{P}\tilde{H}_1\mathcal{P}]_{3,3} = 0 \quad (\text{A.7})$$

and

$$E_2 = [\mathcal{P}\tilde{H}_1\mathcal{Q}\mathcal{R}_0\mathcal{Q}\tilde{H}_1\mathcal{P}]_{3,3} = -\frac{(\gamma_e + 2i\Delta_r)\Omega_r^2}{4\Delta_r(\gamma_e + 2i\Delta_r) - 2i\Omega_e^2}. \quad (\text{A.8})$$

Here, the  $[A]_{i,j}$  indicates the  $i$ -th row and  $j$ -th column element of the matrix  $A$  and  $\mathcal{R}_0 = (E_0\mathbf{1} - \mathcal{Q}H_0\mathcal{Q})^{-1}$  is the so called resolvent. Up to second order in  $\Omega_r$ ,  $\lambda_3$  can be approximated with

$$\lambda_3 = \sum_{n=0}^{\infty} E_n \simeq E_0 + E_1 + E_2 = -\Delta_r - \frac{\Omega_r^2(i\gamma_e - 2\Delta_r)}{8\Delta_r^2 - 2\Omega_e^2 - 4i\gamma_e\Delta_r}. \quad (\text{A.9})$$

We can now calculate the first-order correction to  $|r\rangle$  originated by the other two eigenstates of  $\tilde{H}_0$ ,  $|-\rangle$  and  $|+\rangle$ , both mixed to  $|r\rangle$  by the transformed perturbation Hamiltonian  $\tilde{H}_1$ . For example, the eigenvector  $|u_3\rangle$  associated to  $\lambda_3$ , is:

$$\begin{aligned} |u_3\rangle = & |r\rangle + \frac{\langle -|\tilde{H}_1|r\rangle}{-\Delta_r - E_m} + \frac{\langle +|\tilde{H}_1|r\rangle}{-\Delta_r - E_p} = |r\rangle - \frac{\Omega_r(i\gamma_e - 2\Delta_r)}{2i\gamma_e\Delta_r - 4\Delta_r^2 + \Omega_e^2} |g\rangle + \\ & - \frac{\Omega_e\Omega_r}{2i\gamma_e\Delta_r - 4\Delta_r^2 + \Omega_e^2} |e\rangle. \end{aligned} \quad (\text{A.10})$$

As stated in the main text, the coefficients  $c_n$  can be calculated from the initial condition. For example, setting  $|\psi(0)\rangle = |g\rangle$ , we get

$$c_3 = \frac{\Omega_r(i\gamma_e - 2\Delta_r)}{4\Delta_r^2 - \Omega_e^2 - 2i\gamma_e\Delta_r}. \quad (\text{A.11})$$

## Appendix B. Quantum trajectory simulation algorithm

Here we describe the algorithm of the quantum jump method for a single atom. A generalization for the many-body case is straightforward.

- (i) Prepare the system in a certain (normalized) state  $|\tilde{\psi}(t_0)\rangle_\alpha$  at the initial time  $t_0$ .
- (ii) Compute the probability of the occurrence of a quantum jump at  $t_0$  from  $p_\alpha(t_0) = \gamma_e \langle \tilde{\psi}(t_0) | c^\dagger c | \tilde{\psi}(t_0) \rangle_\alpha dt \ll 1$ , where  $dt$  is an ideally infinitesimal time step. The corresponding probability of no quantum jump is  $1 - p_\alpha(t_0) \approx 1$ .
- (iii) According to these probabilities, randomly choose a no jump/jump event.
- (iv) In case of no jump, propagate  $|\tilde{\psi}(t_0)\rangle_\alpha$  with  $H_{\text{eff}}$  to obtain the normalised wavefunction  $|\tilde{\psi}(t_0 + dt)\rangle_\alpha = e^{-iH_{\text{eff}}dt} |\tilde{\psi}(t_0)\rangle_\alpha / \|\dots\| = (1 - iH_{\text{eff}}dt) |\tilde{\psi}(t_0)\rangle_\alpha / \|\dots\|$ . Otherwise, project the wave function into the ground-state,  $|\tilde{\psi}(t_0 + dt)\rangle_\alpha = \sqrt{\gamma_e} c |\tilde{\psi}(t_0)\rangle_\alpha / \|\dots\| = |g\rangle$ .
- (v) Repeat the procedure from (i) to (iv), until the desired final trajectory time  $t_{\text{max}}$  is reached.

## Appendix C. Steady state Rydberg population

The steady state solution of the single atom master equation can be obtained setting  $\dot{\rho}(t) = 0$  in Eq. (3) of the main text. This is equivalent to calculate the kernel of the matrix of the corresponding optical Bloch equations

$$\frac{\partial}{\partial t} \rho = \begin{pmatrix} -\frac{\gamma_e}{2} & 0 & -i\frac{\Omega_e}{2} & i\frac{\Omega_e}{2} & 0 & 0 & 0 & -i\frac{\Omega_r}{2} & 0 \\ 0 & -\frac{\gamma_e}{2} & i\frac{\Omega_e}{2} & -i\frac{\Omega_e}{2} & 0 & 0 & 0 & 0 & i\frac{\Omega_r}{2} \\ -i\frac{\Omega_e}{2} & i\frac{\Omega_e}{2} & -\gamma_e & 0 & 0 & 0 & 0 & 0 & 0 \\ i\frac{\Omega_e}{2} & -i\frac{\Omega_e}{2} & \gamma_e & 0 & i\frac{\Omega_r}{2} & -i\frac{\Omega_r}{2} & 0 & 0 & 0 \\ 0 & 0 & 0 & i\frac{\Omega_r}{2} & 0 & 0 & -i\frac{\Omega_r}{2} & 0 & -i\frac{\Omega_e}{2} \\ 0 & 0 & 0 & -i\frac{\Omega_r}{2} & 0 & 0 & i\frac{\Omega_r}{2} & i\frac{\Omega_e}{2} & 0 \\ 0 & 0 & 0 & 0 & -i\frac{\Omega_r}{2} & i\frac{\Omega_r}{2} & 0 & 0 & 0 \\ -i\frac{\Omega_r}{2} & 0 & 0 & 0 & 0 & i\frac{\Omega_e}{2} & 0 & -\frac{\gamma_e}{2} & 0 \\ 0 & i\frac{\Omega_r}{2} & 0 & 0 & -i\frac{\Omega_e}{2} & 0 & 0 & 0 & -\frac{\gamma_e}{2} \end{pmatrix} \rho, \quad (\text{C.1})$$

where  $\rho = (\rho_{eg}, \rho_{ge}, \rho_{ee}, \rho_{gg}, \rho_{rg}, \rho_{gr}, \rho_{rr}, \rho_{er}, \rho_{re})^T$ ,  $\rho_{\alpha\beta} = \langle \alpha | \rho | \beta \rangle$  and  $\alpha, \beta = g, e, r$ . (Here, we have suppressed the explicit time dependence of all terms, i.e.  $\rho_{\alpha\beta} \equiv \rho_{\alpha\beta}(t)$  in order to improve the readability.) Since the matrix in Eq. (C.1) is singular, we have an infinite number of steady state solutions parametrized by the (non-normalized) vector

$$\rho(t \rightarrow \infty) = \left( i\frac{\gamma_e}{\Omega_r}, -i\frac{\gamma_e}{\Omega_r}, \frac{\Omega_e}{\Omega_r}, \frac{\gamma_e^2 + \Omega_e^2 + \Omega_r^2}{\Omega_e \Omega_r}, 0, 0, \frac{\gamma_e^2 + \Omega_r^2}{\Omega_e \Omega_r}, 1, 1 \right)^T. \quad (\text{C.2})$$

Using the property of trace conservation of  $\rho(t)$ ,  $\text{Tr}\{\rho(t)\} = \rho_{gg}(t) + \rho_{ee}(t) + \rho_{rr}(t) = 1$ , the normalized steady state Rydberg population can finally be written as

$$\rho_{rr}(t \rightarrow \infty) = \frac{\gamma_e^2 + \Omega_r^2}{2(\gamma_e^2 + \Omega_e^2 + \Omega_r^2)}. \quad (\text{C.3})$$

Notice that Eq. (C.3) converges, for  $\Omega_r \ll \Omega_e, \gamma_e$ , to the equilibrium concentration of Rydberg excitations  $d_{\text{eq}}$  [Eq. (27) in the main text].

## References

- [1] K. Binder and W. Kob, *Glassy Materials and Disordered Solids*, World Scientific, Singapore (2011).
- [2] W. Götze, *Complex Dynamics of Glass-Forming Liquids*, International Series of Monographs on Physics, Oxford University Press (2008).
- [3] P. G. Debenedetti and F. H. Stillinger, *Nature* **410**, 259 (2001).
- [4] L. Berthier and G. Biroli, *Rev. Mod. Phys.* **83**, 587 (2011).
- [5] D. Chandler and J. P. Garrahan, *Ann. Rev. Phys. Chem.* **61**, 191 (2010).
- [6] M. Mézard, G. Parisi, and M. A. Virasoro, *Spin glass theory and beyond*, Singapore, World Scientific, (1987).
- [7] K. Binder and A. P. Young, *Rev. Mod. Phys.* **58**, 801 (1986).
- [8] S. F. Edwards and P. W. Anderson, *J. Phys. F: Met. Phys.* **5** 965, (1975).
- [9] E. Farhi, J. Goldstone, S. Gutmann, J. Lapan, A. Lundgren, D. Preda, *Science* **20**, 5516 (2001).
- [10] T.F. Ronnow, Z. Wang, J. Job, S.V. Isakov, D. Wecker, J.M. Martinis, D.A. Lidar, and M. Troyer, *Science* **345**, 420 (2014).
- [11] P. W. Anderson, *Phys. Rev.* **109**, 1492 (1958).
- [12] D. M. Basko, I. L. Aleiner, and B. L. Altshuler, *Ann. Phys.* **321**, 1126 (2006).
- [13] R. Nandkishore and D. A. Huse, *Annual Review of Condensed Matter Physics*, **6**, 15 (2015).
- [14] A. Pal and David A. Huse, *Phys. Rev. B* **82**, 174411 (2010).
- [15] F. Ritort and P. Sollich, *Adv. Phys.* **52**, 219 (2003).
- [16] H. Shintani and H. Tanaka, *Nature Phys.* **2**, 200 (2006).
- [17] T. E. Markland, J. A. Morrone, B. J. Berne, K. Miyazaki, E. Rabani, and D. R. Reichman, *Nature Physics* **7**, 134137 (2011); W. Lechner and P. Zoller, *Phys. Rev. Lett.* **111**, 185306 (2013).
- [18] B. Olmos, I. Lesanovsky, and J. P. Garrahan, *Phys. Rev. Lett.* **109**, 020403 (2012).
- [19] B. Olmos, I. Lesanovsky, and J. P. Garrahan, *Phys. Rev. E* **90**, 042147 (2014).
- [20] I. Lesanovsky and J. P. Garrahan, *Phys. Rev. Lett.* **111**, 215305 (2013).
- [21] M. Marcuzzi, E. Levi, W. Li, J. P. Garrahan, B. Olmos, and I. Lesanovsky, <http://arxiv.org/pdf/1411.7984v1.pdf> (2014).
- [22] T. F. Gallagher, *Rydberg Atoms*, Cambridge University Press, Cambridge, (1994).
- [23] M. Saffman, T. G. Walker, and K. Mølmer, *Rev. Mod. Phys.* **82**, 2313 (2010).
- [24] T. F. Gallagher, and P. Pillet, *Adv. At. Mol. Opt. Phys.* **56**, 161 (2008).
- [25] C. Ates, T. Pohl, T. Pattard, and J. M. Rost, *Phys. Rev. A* **76**, 013413 (2007).
- [26] H. Weimer, R. Löw, T. Pfau, and H. P. Büchler, *Phys. Rev. Lett.* **101**, 250601 (2008).
- [27] T. Pohl, E. Demler, and M. D. Lukin, *Phys. Rev. Lett.* **104**, 043002 (2010).
- [28] I. Lesanovsky, B. Olmos, and J. P. Garrahan, *Phys. Rev. Lett.* **105**, 100603 (2010).
- [29] I. Lesanovsky, *Phys. Rev. Lett.* **106**, 025301 (2011).
- [30] S. Ji, C. Ates, and I. Lesanovsky, *Phys. Rev. Lett.* **107**, 060406 (2011).
- [31] C. Ates and I. Lesanovsky, *Phys. Rev. A* **86**, 013408 (2012).
- [32] M. Hönig, D. Muth, D. Petrosyan, and M. Fleischhauer, *Phys. Rev. A* **87**, 023401 (2013).
- [33] D. Petrosyan, M. Hönig, and M. Fleischhauer, *Phys. Rev. A* **87**, 053414 (2013).
- [34] D. Petrosyan, *Phys. Rev. A* **88**, 043431 (2013).
- [35] D. W. Schönleber, M. Gärttner, and J. Evers, *Phys. Rev. A* **89**, 033421 (2014).
- [36] A. W. Glätzle, M. Dalmonte, R. Nath, C. Gross, I. Bloch, and P. Zoller, *Phys. Rev. Lett.* **114**, 173002 (2015).
- [37] P. Schauß, M. Cheneau, M. Endres, T. Fukuhara, S. Hild, A. Omran, T. Pohl, C. Gross, S. Kuhr and I. Bloch, *Nature* **491**, 87 (2012).
- [38] G. Günter, M. Robert-de-Saint-Vincent, H. Schempp, C. S. Hofmann, S. Whitlock, and M. Weidemüller, *Phys. Rev. Lett.* **108**, 013002 (2012).

- [39] C. S. Hofmann, G. Günter, H. Schempp, M. Robert-de-Saint-Vincent, M. Gärttner, J. Evers, S. Whitlock, and M. Weidemüller, *Phys. Rev. Lett.* **110**, 203601 (2013).
- [40] M. Robert-de-Saint-Vincent, C. S. Hofmann, H. Schempp, G. Günter, S. Whitlock, and M. Weidemüller, *Phys. Rev. Lett.* **110**, 045004 (2013).
- [41] H. Schempp, G. Günter, M. Robert-de-Saint-Vincent, C. S. Hofmann, D. Breyel, A. Komnik, D. W. Schnöleber, M. Gärttner, J. Evers, S. Whitlock, and M. Weidemüller, *Phys. Rev. Lett.* **112**, 013002 (2014).
- [42] N. Malossi, M. M. Valado, S. Scotto, P. Huillery, P. Pillet, D. Ciampini, E. Arimondo, and O. Morsch, *Phys. Rev. Lett.* **113**, 023006 (2014).
- [43] M. M. Valado, N. Malossi, S. Scotto, D. Ciampini, E. Arimondo, and O. Morsch, *Phys. Rev. A* **88**, 045401 (2013).
- [44] T. M. Weber, M. Höning, T. Niederprüm, T. Manthey, O. Thomas, V. Guarrera, M. Fleischhauer, G. Barontini and H. Ott, *Nat. Phys.* **11**, 157 (2015).
- [45] D. Jaksch, J. I. Cirac, P. Zoller, S. L. Rolston, R. Côté, and M. D. Lukin, *Phys. Rev. Lett.* **85**, 2208 (2000); M. D. Lukin, M. Fleischhauer, R. Côté, L. M. Duan, D. Jaksch, J. I. Cirac, and P. Zoller, *Phys. Rev. Lett.* **87**, 037901 (2001). E. Urban, T. A. Johnson, T. Henage, L. Isenhower, D. D. Yavuz, T. G. Walker and M. Saffman, *Nature Physics* **5**, 110 (2009); A. Gaëtan, Y. Miroshnychenko, T. Wilk, A. Chotia, M. Viteau, D. Comparat, P. Pillet, A. Browaeys and P. Grangier, *Nat. Phys.* **5**, 115 (2009).
- [46] K. D. Nelson, X. Li, and D. S. Weiss, *Nat. Phys.* **3**, 556 (2007).
- [47] Y. O. Dudin and A. Kuzmich, *Science* **336**, 887 (2012).
- [48] F. Nogrette, H. Labuhn, S. Ravets, D. Barredo, L. Bguin, A. Vernier, T. Lahaye, and A. Browaeys, *Phys. Rev. X* **4**, 021034 (2014).
- [49] M. Schlosser, S. Tichelmann, J. Kruse, and G. Birkl, *Quantum Inf. Process* **10**, 907 (2011).
- [50] A. Abdelrahman, M. Vasiliev, K. Alameh, and P. Hannaford, *Phys. Rev. A* **82**, 012320 (2010).
- [51] V. Y. F. Leung, D. R. M. Pijn, H. Schlatter, L. Torralbo-Campo, A. L. La Rooij, G. B. Mulder, J. Naber, M. L. Soudijn, A. Tauschinsky, C. Abarbanel, B. Hadad, E. Golan, R. Folman and R. J. C. Spreeuw, *Rev. Sci. Instrum.* **85**, 053102 (2014).
- [52] J. Billy, V. Josse, Z. Zuo, A. Bernard, B. Hambrecht, P. Lugan, D. Clément, L. Sanchez-Palencia, P. Bouyer and A. Aspect, *Nature* **453**, 891 (2008).
- [53] G. Roati, C. D'Errico, L. Fallani, M. Fattori, C. Fort, M. Zaccanti, G. Modugno, M. Modugno and M. Inguscio, *Nature* **453**, 895 (2008).
- [54] C. W. Gardiner and P. Zoller, *Quantum noise*, 3rd Edition, Springer-Verlag, Berlin Heidelberg (2004).
- [55] T. E. Lee and M. C. Cross, *Phys. Rev. A* **85**, 063822 (2012).
- [56] J. Dalibard, Y. Castin, and K. Mølmer, *Phys. Rev. Lett.* **68**, 580 (1992).
- [57] R. Dum, P. Zoller, and H. Ritsch, *Phys. Rev. A* **45**, 4879 (1992).
- [58] D. T. Pegg and P. L. Knight, *Phys. Rev. A* **37**, 4303 (1988).
- [59] C. Cohen-Tannoudji and J. Dalibard, *Europhys. Lett.*, **1**, 441 (1986).
- [60] M. B. Plenio and P. L. Knight, *Rev. Mod. Phys.* **70**, 101 (1998).
- [61] G. H. Fredrickson and H. C. Andersen, *Phys. Rev. Lett.* **53**, 13 (1984).
- [62] G. H. Fredrickson and H. C. Andersen, *J. Chem. Phys.* **83**, 5822 (1985).
- [63] R. J. Glauber, *J. Math. Phys.* **4**, 294 (1963).
- [64] S. Léonard, P. Mayer, P. Sollich, L. Berthier, and J. P. Garrahan, *J. Stat. Mech.*, P07017 (2007).
- [65] A. W. Glaetzle, R. Nath, B. Zhao, G. Pupillo, and P. Zoller, *Phys. Rev. A* **86**, 043403 (2012).
- [66] I. I. Beterov, I. I. Ryabtsev, D. B. Tretyakov, and V. M. Entin, *Phys. Rev. A* **79**, 052504 (2009).
- [67] K. C. Younge, B. Knuffman, S. E. Anderson, and G. Raithel, *Phys. Rev. Lett.* **104**, 173001 (2010).
- [68] S. D. Hogan and F. Merkt *Phys. Rev. Lett.* **100**, 043001 (2008).
- [69] R. Mukherjee, J. Millen, R. Nath, M. P. A. Jones and T. Pohl, *J. Phys. B: At. Mol. Opt. Phys.* **44**, 184010 (2011).
- [70] J. R. Johansson, P. D. Nation, and F. Nori, *Comp. Phys. Comm.* **184**, 1234 (2013).